FAILURE ANALYSIS OF A WELDED MOMENT-RESISTING INTERIOR CONNECTION

By
John. M. Barsom
and
James V. Pellegrino Jr.

Submitted to:
AISC
Chicago, IL

September 15, 2001

FAILURE ANALYSIS OF A WELDED MOMENT-RESISTING INTERIOR CONNECTION

by
John M. Barsom[1]
James V. Pellegrino, Jr.[2]

INTRODUCTION

Two full-scale welded moment-resisting interior connections were tested at the University of Minnesota (UM). The connection, designated CR-4, fractured prematurely under simulated earthquake cyclic loads. The connection was fabricated with two W24 x 94 beams and a W14 x 176 column. The panel zone of the column was stiffened with two 3/4-inch doubler plates. The doubler plates were placed about 2 inches on either side of the web. The doubler plates were joined to the column flanges by using complete joint penetration (CJP) groove welds.

The connection details are presented in Figures 1 through 3 (Dexter, 2001-b). The CJP groove welds joining the beam flanges and the column were made by using a 5/64-inch diameter E70T-6 electrode (Lincoln NR-305), a Miller inverter power supply, and a Lincoln LN-25 wire feeder. The welding parameters used to fabricate the connection are presented in Table 1. The shear tab welds to the column flange and to the webs of the beams, and the reinforcing fillet welds were made with an E71T-8 electrode (Lincoln NR-232).

---

[1] Barsom Consulting, Ltd., 1316 Murray Avenue, Suite 300, Pittsburgh, PA 15217
[2] WHEMCO, West Seventh Avenue, Homestead, PA 15120

Three of the four beam-to-column flange welds in connection CR-4 fractured in a brittle

manner. Yielding of the beam flanges occurred prior to fracture, initiating during the 0.75% drift cycle (Dexter 1001-a). The first visible crack was noticed in the top flange of the east beam (ET) after the first quarter cycle at 1.5% drift. The top flange of the west beam (WT) fractured during the second cycle at 1.5% drift. The ET and the bottom flange of the west beam (WB) fractured during the first cycle at 2.0% drift. The weld joining the bottom flange of the east beam (EB) was not fractured when the test was terminated.

UM fabricated and tested a connection that was designated CR-1. This connection had a different design and configuration from the CR-4 connection. It had an unstiffened W14 x 283 column and two W24 x 94 beams. The CJP groove welds joining the beam flanges and the column were made by using the same 5/64-inch diameter E70T-6 (Lincoln NR-305) electrode as for the CR-4 connection. The shear tab welds to the column flange and to the webs of the beams, and the reinforcing fillet welds were made with the same E71T-8 (Lincoln NR-232) electrode as for the CR-4 connection.

The welding equipment and welding parameters that were used to weld the CR-1 connection are presented in Table 1. A comparison of the information presented in Table 1 shows that the CR-4 and the CR-1 were welded with different power supplies and under significantly different currents. The CR-1 connection, unlike the CR-4 connection which fractured prematurely, achieved three to four cycles at 4% interstory drift before any cracks were observed. Also, weld metal impact Charpy V-notch (CVN)

tests that were conducted subsequent to cyclic loading resulted in 2 ft-lb at 0°F and at 70°F for the CR-4 connection and 2 ft-lb and 19 ft-lb at 0°F and at 70°F for the CR-1 connection

AISC initiated two studies to determine the cause of the premature fracture in connection CR-4. One study was conducted by Dr. Matt Johnson of EWI to determine weld-metal diffusible-hydrogen concentration, to evaluate the weld metal microstructure and to determine the origin of the apparent difference in the chemical composition between the deposited E70T-6 weld metal in connection CR-4 and in other connections that performed satisfactorily under similar loading conditions (Johnson, 2001). The present report presents the results of the second study which was a metallographic and fractographic investigation of the three fracture CJP groove welds joining the beam flanges and the column flanges in connection CR-4.

EXPERIMENTAL WORK AND TEST RESULTS

Beam and column samples that contained the fracture surfaces of the three fractured joints were removed from the tested CR-4 connection and were sent to Barsom Consulting, Ltd. for further study. The study determined the chemical composition of the beam, the column and the deposited weld metal, and the microstructure of the deposited weld metal. Metallographic and fractographic investigations were conducted on the three joints that fractured during cyclic loading. The results of the study are presented in the following sections.

Chemical Composition

Base metal and weld metal samples from connection CR-4 were sent to EWI for chemical analysis. The results of the analysis are presented in Table 2. The alloy content of the beam and of the column was typical of the product. The alloy content of the 5/64-in.-diameter E70T-6 deposited weld metal fell within the composition range specified by AWS A5.20.95. The Lincoln Electric Company confirmed that the alloy content of the deposited weld metal were consistent with the composition of the 5/64-in.-diameter wire supplied prior to 1998. The effects of alloy content on weld-metal properties have been discussed by Johnson (2001).

Microstructure

The microstructure of the deposited weld metal is shown in Figures 4 and 5. The micrographs in Figure 4 show the as-deposited solidification microstructure within a deposited weld bead at 50X and 400X magnification. The microstructure within a weld bead was composed of retained delta ferrite, ferrite, and ferrite/carbide aggregate. Figure 5 shows the recrystallized equiaxed ferrite microstructure between passes.

West-Beam Bottom-Flange Joint

Figure 6 shows the fractured WB joint in the test frame. The photographs demonstrate that the bottom flange adjacent to the CJP weld was subjected to forces equal to or higher than the yield stress of the bottom beam flange. The fracture of the joint was along an irregular line, Figure 6-b, which is not typical of a single crack propagating in a brittle manner.

The as received fracture surfaces from the fractured WB joint are shown in Figure 7. Figure 7-a is the fracture surface on the beam side. This sample was sectioned at UM prior to shipping. Figure 7-b is the matching fracture surface on the column flange. Most of the high temperature oxide (HTO) on this fracture surface occurred during thermal cutting the piece from the column flange. The fracture propagated in brittle manner and exhibited a coarse crystalline (cleavage) fracture. The crack propagated, primarily, in the deposited weld metal. At about the mid-length of the CJP groove weld, the fracture surface revealed large slag inclusion, porosity and lack of fusion.

The letters and numbers on the pieces shown in Figure 7 were placed by the UM researchers. The markings in this and in other figures identify the pieces as: east beam (E), west beam (W), top flange (T), north end (N), south end (S), a center section (C), macro section (M) and samples 1 and 2. These designations are used herein, when needed, to avoid confusion.

The south, center and north pieces from the fracture surfaces on the beam side of the WB connection are presented in Figures 8, 9, and 10, respectively. The fracture surface in Figure 8 shows the presence of a few transverse cracks that are oriented at different angles to the deposited weld metal. The figure shows also two longitudinal cracks that have HTO on their surfaces. The fracture surface at mid-length of the CJP weld, Figure 9, shows a large weld defect, two longitudinal cracks that were covered with HTO, a transverse crack, and several cracks that were parallel to the surface of the deposited weld metal. The fracture surface of the north piece shows a few cracks two of which were longitudinal surface cracks that were covered with HTO.

Fracture of the WB joint initiated at the large weld defect and at the larger HTO covered crack, located within the mid-length of the CJP groove weld. The fracture was, primarily, in the deposited weld metal. The fracture initiated and propagated, primarily, in a brittle manner by cleavage and exhibited coarse crystalline features. Figure 11 presents two examples of ductile fractures by void coalescence that were observed in a few areas on the fracture surface of the WB joint.

Cross Sections

Polished and etched cross sections through the CJP groove weld of the WB joint are shown in Figure 12. Very few cracks are visible on the surface of the cross section.

Figure 13-a is a polished and etched section through the column flange, the CJP groove weld and the west bottom flange. The macro section indicated that the crack propagated in the E70T-6 deposited weld metal and along the fusion plane between the reinforced fillet and the beam flange. The crack did not propagate into the E71T-8 (Lincoln NR-232) deposited weld metal of the reinforcing fillet. The amount of back gouging and the large depth, the large volume and the number of weld passes of the reinforced fillet, were unexpected.

The macro section in Figure 13-a had two small areas that contained very small cracks. The cracks in these two areas are shown in Figures 13-b and 13-c. Some of the cracks appeared to be along solidification grain boundaries, while other cracks crossed the solidification grain boundaries at various angles. The semi-circular crack in Figure 13-c intersected the solidification grain boundaries within a single weld pass at 90 degrees. The cracks in Figures 13-b and 13-c were studied at increasing

magnifications. The cracks in Figure 13-c that are in the vicinity of the semi-circular cracks are presented in Figures 14 and 15. These figures show cracks that propagated perpendicular to each other in steps and cracks that appear to propagate in a random manner. The black areas in Figure 14 are locations where small pieces of the weld metal were surrounded by cracks causing them to fall out of the polished and etched surface. Figure 15 shows the crystallographic planes of ferrite that extended from the end of the cracks or that were perpendicular to the cracks. Figures 14 and 15 show clusters of intersecting crystallographic planes of ferrite that had not yet developed into cracks when the joints fractured.

The two perpendicular cracks in the area marked C in Figure 14 are presented in Figure 16 at higher magnifications. Figure 16-a shows that the cracks were discontinuous and that some of the crack segments contained particles. The particles could have caused crack initiation within these segments. Most crack segments investigated, however, did not contain particles. The crack on the left side in Figure 16-a and 16-b deviated temporarily from a straight-line path to propagate along the boundary of a microstructural obstacle. Both ends of this crack had very fine cracks that were in the process of coalescing with the larger cracks. This feature and the presence of crystallographic planes of ferrite at different stages of development to becoming cracks, Figure 17, demonstrate that the cracks shown in Figure 13 initiated and propagated during cyclic loading of the joint.

Figures 18-a, 18-b and 18-c show a cluster of intersecting crystallographic planes at 250X, 500X and 1000X magnifications, respectively. These planes which appear to be innocuous at 250X and at 500X magnifications, appear at 1000X magnification to be

the birth location of cracks. Under further cyclic loading this cluster of planes would have developed into an intersecting network of cracks. This was the origin of the network of cracks shown in Figure 13 and the crack that caused the fracture of the WB joint. The crystallographic planes did not show any evidence of plastic deformation.

East-Beam Top-Flange Joint

Figure 19 shows the fractured ET joint in the test frame. The photographs demonstrate that the beam adjacent to the CJP groove weld was subjected to forces equal to or higher than the yield stress of the base metal. The fracture of the joint was along a meandering line that is not characteristic of a single crack propagating in a brittle manner.

Fracture Surfaces

The as received fracture surfaces from the ET joint are shown in Figure 20. Figure 20-a is the fracture surface on the beam side. This sample was sectioned at UM prior to shipping. Figure 20-b is the matching fracture surface on the column flange.

The south, center and north pieces from the fracture surface on the beam side are represented in Figures 21, 22 and 23, respectively. These figures show the presence of a few cracks that were oriented along, transverse, through thickness and inclined to the CJP groove weld. The cracks occurred at various depths from the root pass to the top passes of the deposited weld metal. Some of the cracks formed at high temperatures. The surfaces of these cracks were covered with HTO. Figure 24 is another view of the center piece. It shows a wedge of weld metal that was separated

from the beam-side fracture surface. Figure 20 shows this piece to be attached to the column-side of the fracture. This piece was formed by cracks that were present in the weld metal prior to fracture of the joint. The cracks initiated from a lack-of-fusion defect between the root pass and the backing bar and propagated into each subsequent weld pass up to the surface of the deposited weld metal. Crack propagation occurred at high temperatures as each deposited weld pass was cooling. The cracks propagated along and transverse to the deposited weld metal and intersected at about 90 degrees on the weld surface. An extension of one of the transverse cracks that formed the wedge is visible in Figure 24. The north piece of the beam-side fracture surface, Figures 23, shows a lack-of-fusion defect between the backing bar and the root pass and between the root pass and the subsequent pass.

The fracture surfaces in Figures 21 through 23 show some areas having a rough texture and some areas having a smooth texture. These figures and Figure 20 show that the fracture of the ET joint occurred, primarily in the smooth-textured area. Further analysis demonstrated that the rough-texture fracture was in the weld metal and the smooth-texture fracture was in the fusion plane between the weld metal and the column flange. Thus, the fusion plane was the region least resistant to the fracture under the applied load and deformations. Further evidence of crack propagation along the fusion plane is presented in the next section.

Figure 25 shows an area of the fracture surface at a boundary between weld-metal and fusion-plane fracture surfaces. The features on the fracture surface in the weld metal demonstrate that the crack propagated in a brittle manner by cleavage. The mode of crack propagation along the fusion plane are not clear at this magnification.

At higher magnification, the fractographs in Figure 26 demonstrate that the fracture propagated along the fusion plane, also, in a brittle manner by cleavage.

The fracture surfaces of the ET joint indicated that the fracture initiated at multiple locations from pre-existing cracks. Crack propagation was primarily along the fusion plane between the deposited weld metal and the column flange. Except for a few isolated areas that fractured in a ductile manner, the joint fractured in a brittle manner by cleavage.

Cross Sections

Polished and etched macro cross-sections through the CJP groove weld of the ET joint are presented in Figure 27. The cross sections show the presence of a few cracks that are at different orientations to the CJP groove weld. Figure 28-a shows a polished and etched surface of a macro cross section through the column flange, the deposited weld metal and the beam flange. This macro section was formed by gluing two matching fracture surfaces. The cross section demonstrates that the fracture was primarily along the fusion plane. Figure 28-b presents an example of pre-existing cracks in the ET joint. Two of the cracks were about 0.1-inch long; the other two cracks were about an order of magnitude shorter. One crack extended from the toe of the root pass on the beam flange, the other three were along solidification grain boundaries. The cracks shown in Figure 27 were longer than those in Figure 28-b and propagated along and transverse to the solidification grain boundaries.

A close examination of the fracture path in Figure 28-a demonstrated that the crack propagated along the fusion plane between the deposited weld metal and the column

flange. The features along the fracture path demonstrated that the crack initiated from the top of the deposited CJP groove weld towards the backing bar. These features are demonstrated in Figure 29 which is a close-up of the fracture initiation region corresponding to the upper right hand corner of the CJP groove weld in Figure 28-a.

West-Beam Top-Flange Joint

Figure 30 shows the fractured WT joint in the test frame. The photographs demonstrate that the beam flange adjacent to the CJP groove weld was subjected to forces equal to or higher than the yield stress of the beam flange. The fracture of the joint was along an irregular line which is not a characteristic of a single crack propagating in a brittle manner.

Fracture Surface

Figure 31 shows the as-received samples of the fracture surfaces from the WT joint. The top samples in the figure were from the fracture surface on the beam side. This sample was sectioned by the UM researchers prior to shipping. The bottom sample is the fracture surface on the column flange. This fracture shows an extensive network of cracks that are at different orientations within the deposited weld metal. The fracture surface indicated that the final fracture propagated along pre-existing cracks in the weld metal then along the fusion plane on the column flange.

The south, center and north pieces of the fracture on the beam side are shown in Figures 32, 33 and 34, respectively. The south piece, Figure 32-a, shows lack-of-fusion defects at the weld root and within the CJP groove weld, and pre-existing cracks. A

crack at the edge of the piece was coated with HTO. Most likely, the HTO formed when the run-on and run-off tabs were removed and the edges of the CJP groove weld were ground smooth.

The center piece, Figure 33-a, shows lack-of-fusion between the root pass and the backing bar and an extensive network of discontinuous cracks. The surfaces of two cracks were coated with HTO. Figure 34 presents an example of the many discontinuous cracks along the crystallographic planes in ferrite that were present on the fracture surface. The figure shows also, that the mode of microscopic crack propagation at this location was a mixture of cleavage and ductile dimples. The north piece, Figure 35-a, shows severe slag and lack-of-fusion defects and cracks that were parallel to the top of the deposited weld metal. Some of these cracks are shown in Figure 35-b at higher magnification.

Figures 32-b and 33-b show the mode of fracture for the center and south pieces, respectively. The fractographs are of randomly selected areas that are representative of the fracture in the weld metal. The primary crack that caused the failure of the WT joint propagated in a brittle manner by cleavage. The fracture initiated in the weld metal then propagated in the weld metal and along the fusion plane.

Cross Sections

Two cross sections of the WT joint are shown in Figures 36. The polished and etched surfaces of the cross sections show the presence of an extensive network of cracks that were present prior to fracture. The cracks were randomly oriented

throughout the weld metal. The fracture path indicated that the fracture propagated along an irregular network of cracks.

Figure 37-a is a macro cross section through the column flange, the CJP groove weld and the west top flange. The features along the fracture path indicated that the fracture propagated from the top surface of the deposited weld metal and along the fusion line into the gap between the backing bar and the column flange. The extensive network of cracks within the weld metal is not clearly visible in this cross section because the cracks were filled with wax to prevent crack "bleeding" from etchant that was entrapped within the cracks. Figure 37-b shows some of the cracks that were present in the weld metal. The weld metal in this WT joint contained significantly more cracks than either the WB or the ET joints.

Figures 38 and 39 present two examples of cracks in cross sections from the WT joint. Figure 38-a shows a step crack that formed along perpendicular crystallographic planes in the ferrite. Crystallographic planes extending from the tips of the step cracks are indicated by arrows in Figure 38-b. Figure 39-a shows a meandering crack that propagated along crystallographic planes of the ferrite. Figure 39-b and 39-c show crystallographic planes at different stages of development towards becoming cracks

Discussion

The deposited weld metal in the CR-4 connection exhibited a coarse microstructure that had low ductility and low fracture toughness. These properties resulted, in part, in the initiation of pre-existing cracks in the deposited weld metal and in the initiation and propagation of cracks along crystallographic planes in the ferrite under cyclic

loading. Although the same 5/64-inch-diameter E70T-6 electrode was used to weld the CR-4 and CR-1 joints, the deposited weld metal in the CR-1 joint did not have the same microstructure (Johnson, 2001) and performed significantly better under cyclic loading than the CR-4 connection (Dexter,2001-a).

The deposited weld metal in the CR-4 connection contained many preexisting cracks and cracks that initiated and propagated during cyclic loading. The cracks were discontinuous and formed along crystallographic planes of ferrite. These cracks had different lengths and depths and intersected the CJP groove weld at different angles. Most cracks in a cross section of the CJP groove welds were eliminated and new ones exposed when the surface was ground a few mils, repolished and etched. Therefore, the size of the cracks along the CJP groove welds was very small. Fracture of a welded joint occurred when the applied loads and displacements exceeded the resistance of the weld metal with discontinuous cracks. The resistance of the weld metal with cracks exceeded the yield strength of the beam flanges as evident from the deformation of the flanges next to the CJP groove welds.

Some crack surfaces were coated with HTO. For the crack surfaces to be coated with HTO, the cracks would have had to be present when the temperature of the surrounding metal reached about 600°F or higher. The HTO coated cracks that were located at the edges of the CJP groove welds occurred, most likely, when the run-on and run-off tabs were removed and the edges were ground smooth. The large pre-existing HTO coated crack in the ET joint initiated at a weld defect between the root pass and the backing bar and extended into subsequent weld passes as the weld metal in each pass solidified and contracted. One of the HTO coated surface cracks in the WB

joint appeared to form in an area on the top surface of the deposited weld metal that had been altered after the top weld pass was deposited, Figure 40. Another HTO surface crack appeared to have originated as a crater crack. The remaining HTO coated cracks could not be investigated within the limits of the present study.

Examination of the fracture surfaces and several macro-section surfaces demonstrated that the WT joint contained significantly more cracks than the ET joint or the WB joint. The three joints fracture at about the same applied load, number of cycles and deformation (Dexter, 2001-b). Thus, difference in crack density could not be related to differences in test conditions.

All four joints in the CR-4 connections were welded with the same small quantity of the 5/64-in.diameter E70T-6 electrode. It is highly unlikely that significant variation of chemical composition would be expected within a particular spool. Thus, the difference in crack density between the WT joint and the other joints could not be related to variability in the electrode composition. Finally, the differences in crack density among the joints could not have been caused by difficulties in welding the WT joint as compared to welding the ET joint or, especially, the WB joint. The only remaining factor that could have caused the difference was the welding parameters. Johnson (2001) reviewed the welding parameters that were used to weld the CR-4 and the CR-1 connections and concluded "that the reported CR-4 parameters were outside the recommended range specified by Lincoln Electric". Under these welding conditions, the deposited weld metal could be sensitive to small variations in the welding parameters. The difference in the cyclic performance of the CR-1 and the CR-4

connections and the difference in cracking density between the WT joint and the other joints in the CR-4 connection are consistent with this observation.

The small quantity of the specified welding electrode used to weld the connections was consumed in welding the connections. Therefore, the relative sensitivity of the electrode to small variation in the welding parameters that are within or outside those recommended by the manufacturer could not be evaluated. Such an investigation on a similar electrode diameter and composition may be of value.

High-strain low-cyclic loads degrade the impact CVN toughness of steel base metals and weld metals. The impact CVN toughness of the deposited weld metal was not determined prior to testing the connection. High-strain low-cycle deformations and the initiation and propagation of discontinuous cracks during testing would have degraded the notch toughness of the weld metal. CVN tests conducted on the EB joint resulted in 2 ft-lb energy absorption at temperatures of 0°F and 70°F. The correspondence between the low values and the notch toughness of the deposited weld metal prior to cyclic loading cannot be established in the absence of additional filler metal from the same E70T-6 electrode and to weld the CR-4 connection.

SUMMARY

1. The chemical composition of the base metal and of the weld metal used for the fabrication of the CR-4 connection were within the ranges specified in the applicable specifications.

2. In spite of the fact that the CR-1 and the CR-4 connections were welded with the same 5/64-inch-diameter E70T-6 electrode, the deposited weld metal in the CR-4 connection, unlike in the CR-1 connection, exhibited coarse microstructure that had low ductility and low fracture toughness.

3. The difference in the microstructure and the cyclic performance of the CR-1 and the CR-4 connections appeared to be related to the relative sensitivity of the 5/64-inch-diameter E70T-6 electrode to the different welding equipment and welding parameters, or both, that were used to weld the connection.

4. Cyclic loading produced discontinuous cracks in the deposited weld metal of the CR-4 connection. The cracks formed along crystallographic planes in the ferrite.

5. The discontinuous cracks that formed in the deposited weld metal of the CR-4 connection during testing intersected the CJP groove weld at various angles.

6. Fracture of each of the three welded joints that fractured in the CR-4 connection occurred when the driving force exceeded the resistance force of the weld metal discontinuous cracks. The level of the driving force was equal to or exceeded the yield stress of the beam flanges.

7. Fracture of the joints in the CR-4 connection were along an irregular plane that was formed by connecting discontinuous, small cracks that had different orientations to the CJP groove weld.

8. Final fracture of the welded joints in the CR-4 connection was, primarily, in a brittle manner by cleavage.

9. The primary cause of premature failure of the welded joints in the CR-4 connection appeared to be related to variations in welding equipment and welding parameters that resulted in low ductility, low toughness and cracking of the weld metal. The relative sensitivity of the 5/64-in.-diameter E70T-6 electrode used to weld the CR-1 and the CR-4 connections to variations in the welding parameters could not be investigated because it was consumed in welding the connection.

10. High-strain low-cyclic loads degrade the impact CVN toughness of steel base metals and weld metals. Consequently, the CVN values measured from the EB joint, that did not fracture when the test was terminated, characterize the impact notch toughness of the cyclically loaded weld metal in the connection. A relationship between these values and the as deposited weld metal does not exist.

RECOMMENDATIONS

1. The relative sensitivity of the 5/64-inch-diameter E70T-6 electrode to different welding equipment and to variations in welding parameters needs to be investigated.
2. The significant parameters, if any, that would be identified in the investigation recommended in Item 1, should be incorporated in the procedure qualification requirements.
3. The effects of the different geometries and configurations used in the design of the CR-1 and CR-4 connections on their cyclic performance need to be investigated further.

REFERENCES

Dexter, R. J. and Hajjar, J. F., "Brief Summary of Results for Cruciform Specimen CR-4," AISC Project #98/47C, February 26, 2001-a.

Dexter, R. J., Hajjar, J. F., Bergson, P. M., Cotton, S. C., Prochnew, S. D. and Ye, Yangun, "Reassessment of Design Criteria and New Alternatives for Column Transverse Stiffeners (Continuity Plates) and Web Double Plates" AISC Project #98/47C, Project Oversight Meeting, March 27, 2001-b.

Johnson, M., "Evaluation of E70T-6 Weld Metal," EWI Project No, 45443CSP, Edison Welding Institute, Columbus, OH, August 9, 2001.

Table 1

Summary of Parameters Used to Weld the CR-1 and Cr-4 Connections

	CR-1	CR-4
Electrode Type	FCAW-S	FCAW-S
Trade Name	NR-305	NR-305
AWS Designation	E70T-6	E70T-6
Electrode Dia. (in.)	5/64	5/64
Electrode Manufacturer	Lincoln	Lincoln
Electrode Code	4N22GSAD	4N22GSAD
Power Supply	Miller Maxtron 450	Miller Inverter
Wire Feeder	Miller S-64	LN-25
Voltage (V)	28.5 - 29.5	29 - 30
WFS (ipm)	380	380
Current (A)	430 - 460 DCEP	330 - 380
Preheat (°F)	150 min	150 min
Interpass (°F)	150 min	150 min
Electrode Extension (in.)	1	1
Travel Speed (ipm)	10 -15	10 - 15

Table 2

Chemical Composition of the Deposited Weld Metal, Beam and Column of the CR-4 Connection, Percent.

Element	Weld	Beam	Column
Carbon	0.076	0.072	0.098
Manganese	0.070	1.21	1.29
Phosphorus	<0.005	0.011	0.008
Sulfur	0.006	0.028	0.027
Silicon	0.28	0.14	0.23
Copper	0.10	0.33	0.32
Nickel	<0.10	0.012	0.013
Chromium	<0.10	<0.10	<0.10
Molybdenum	<0.05	<0.05	<0.05
Titanium	0.19	<0.02	<0.01
Aluminum	0.96	<0.005	<0.005
Niobium	<0.01	<0.01	<0.01
Boron	0.0009	0.0005	0.0008
Nitrogen	0.028	0.012	0.013
Oxygen	0.033	0.0085	0.0067
Cobalt	<0.05	<0.05	<0.05
Tin	<0.01	0.012	0.010
Tantalum	<0.10	<0.10	<0.10
Tungsten	<0.10	<0.10	<0.10
Zirconium	<0.01	<0.01	<0.01

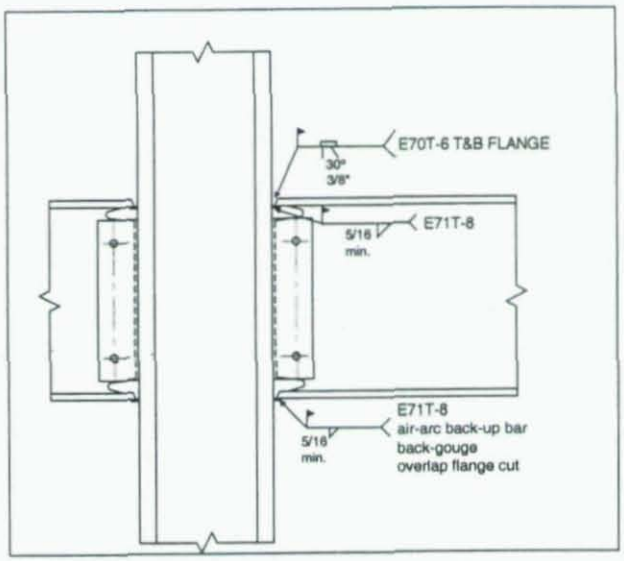

Figure 1. Flange connection details.

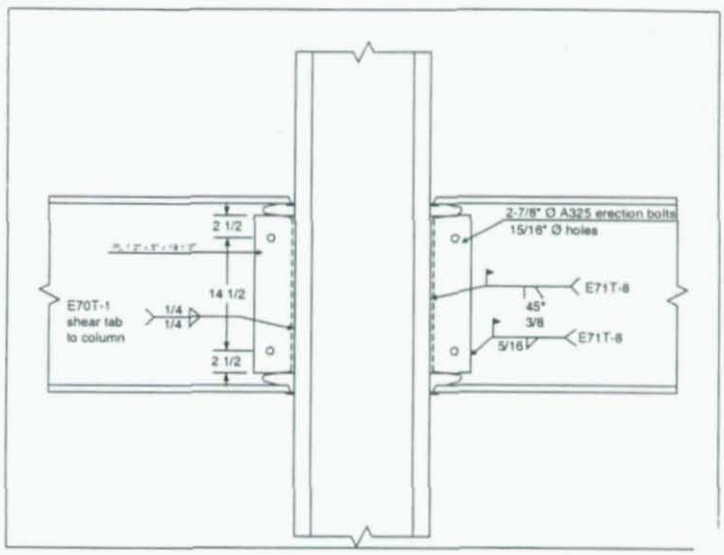

Figure 2. Web connection details.

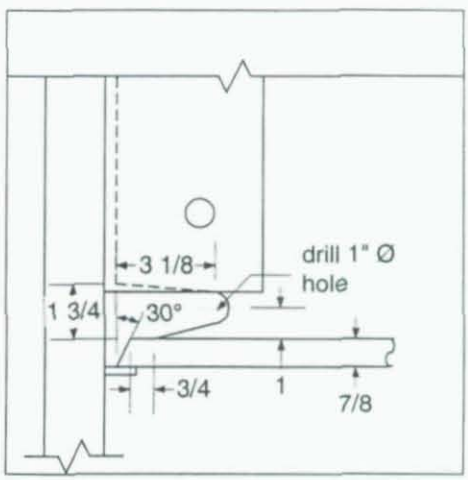

Figure 3. Weld access-hole details.

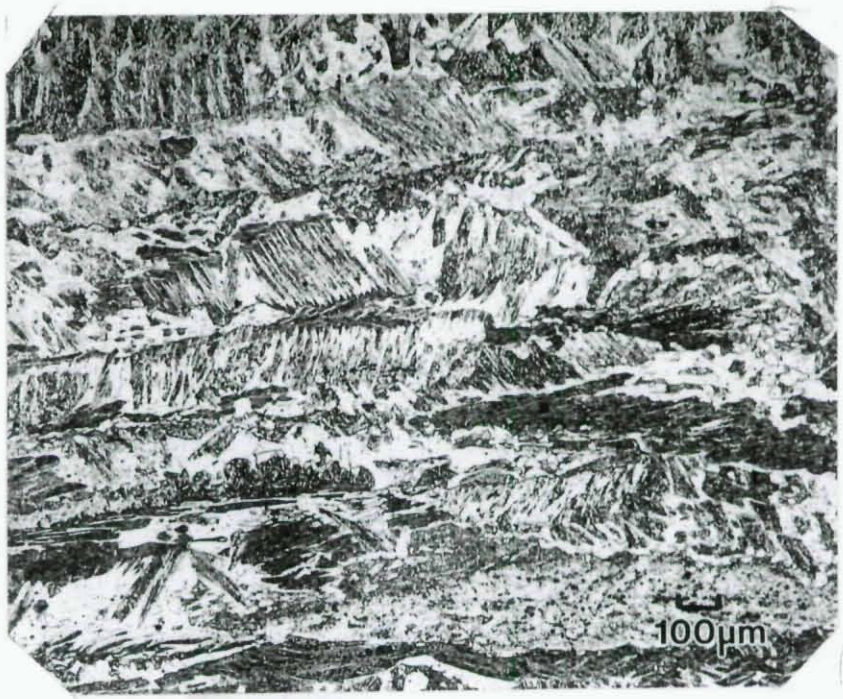

a) 50X magnification

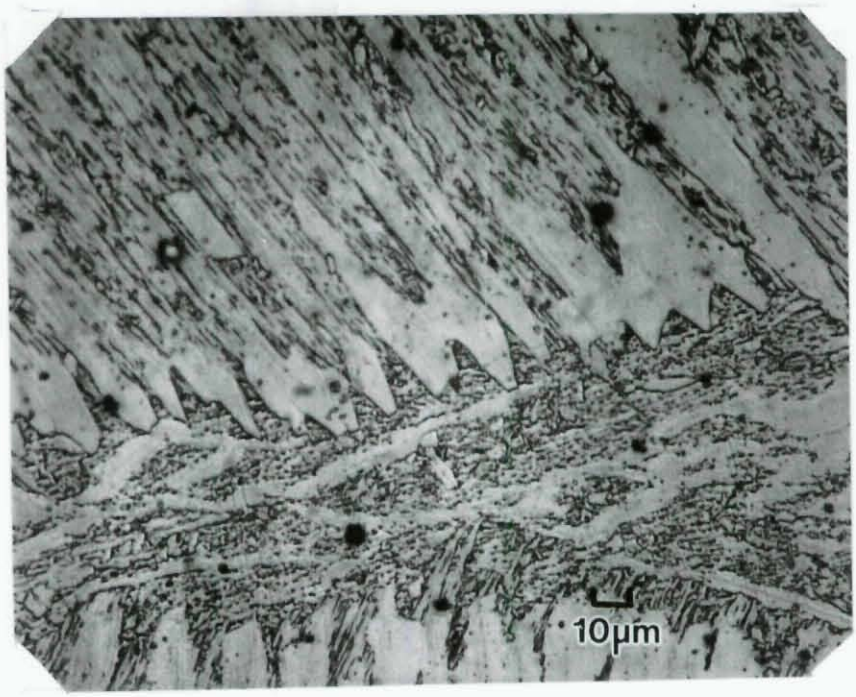

b) 400X magnification

Figure 4. Microstructure within a deposited weld bead.

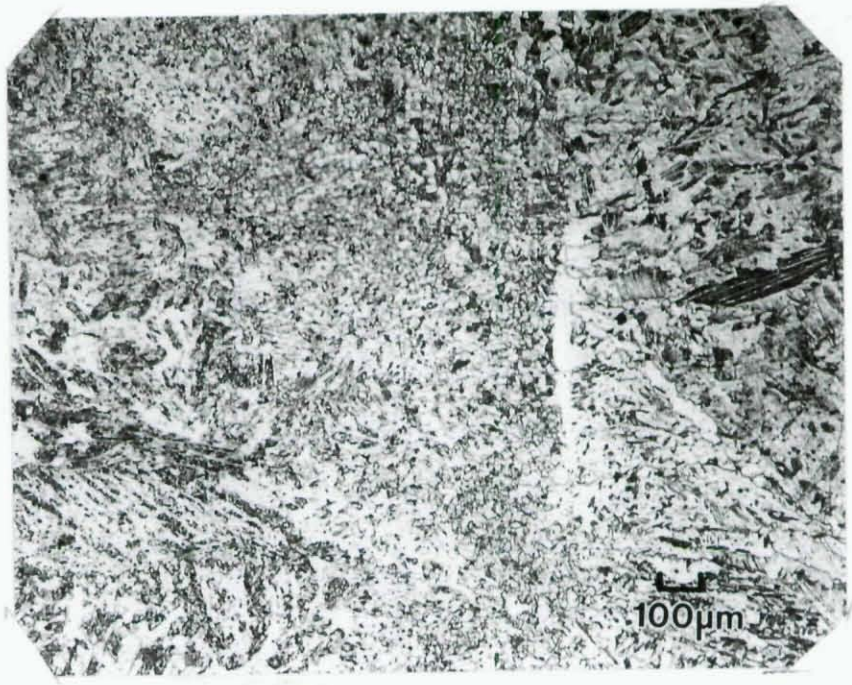

a) 50X magnification

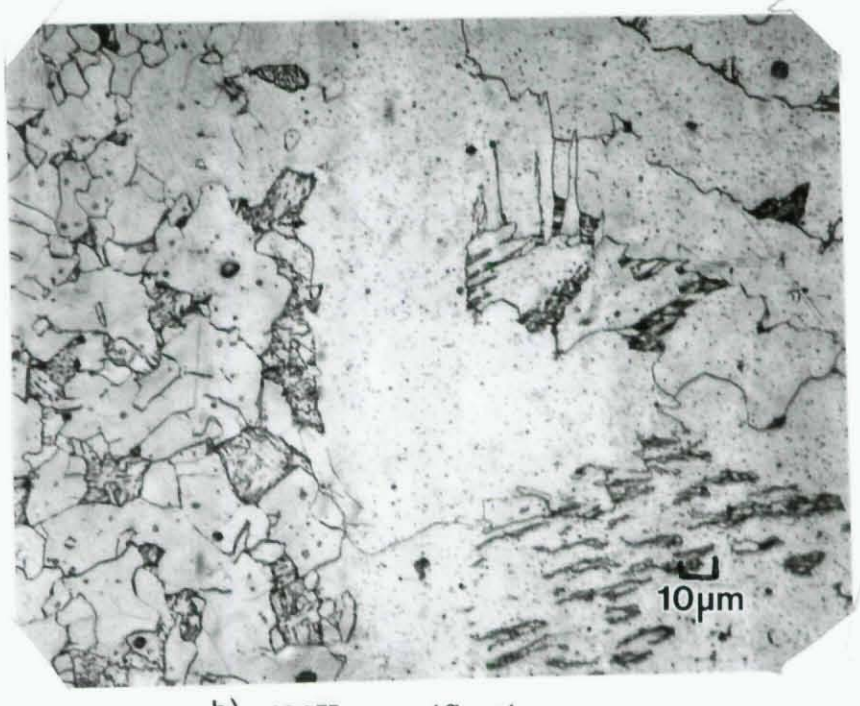

b) 400X magnification

Figure 5. Microstructure between weld beads.

a)

b)

Figure 6. Fractured west-beam bottom flange.

c)

Figure 6. Fractured west-beam bottom flange.

a)

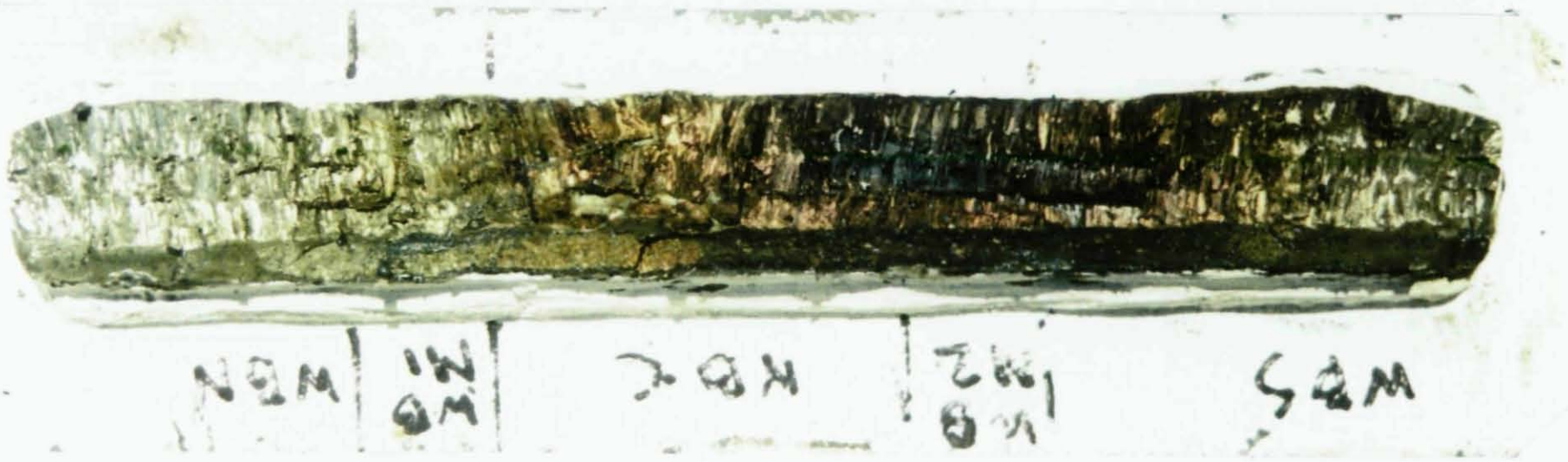

b)

Figure 7. As received fracture pieces from the west-beam bottom-flange joint.

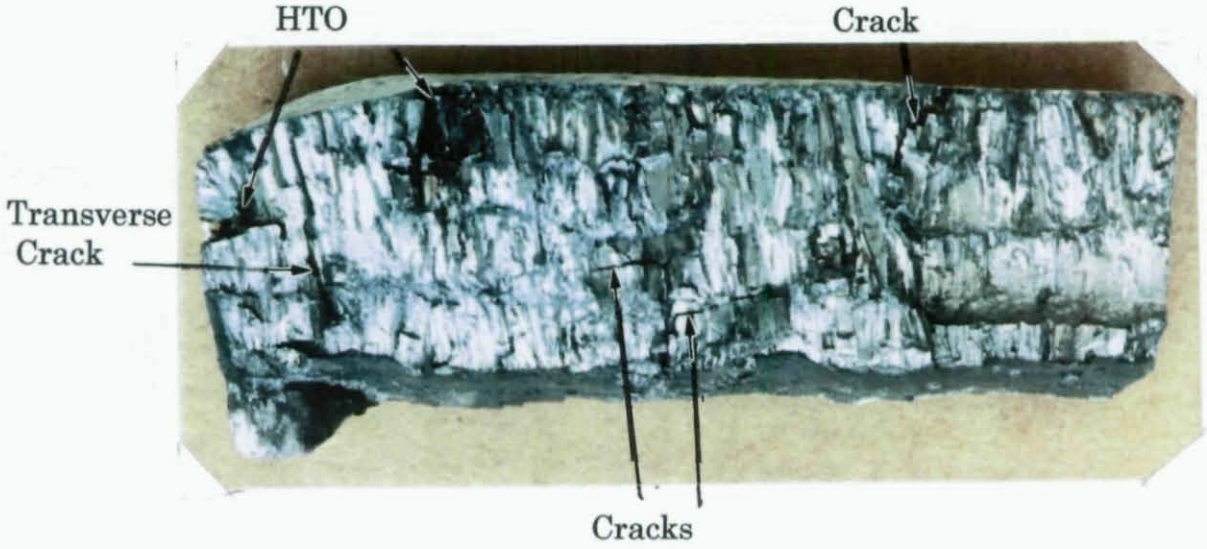

Figure 8. Fracture surface of the south end from the west-beam bottom-flange joint

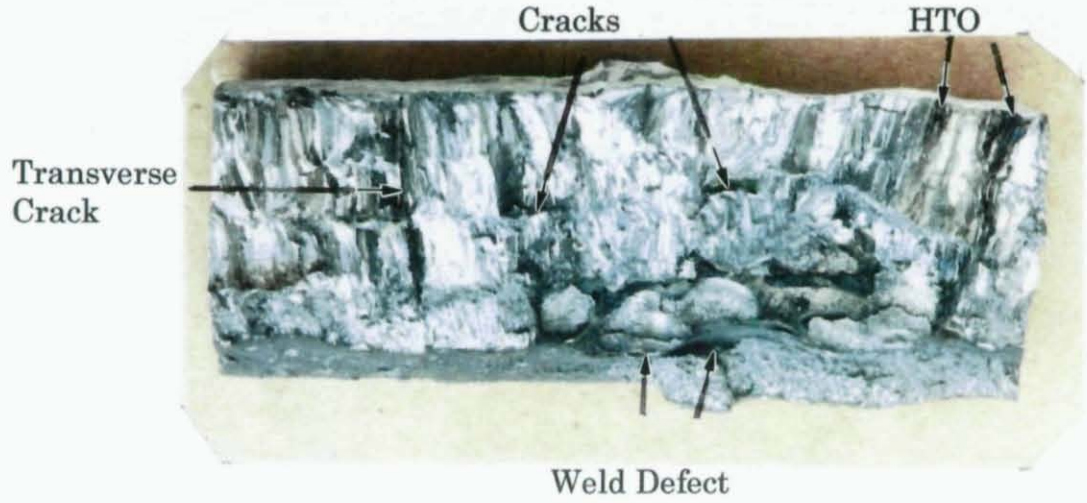

Figure 9. Fracture surface of the center section from the west-beam bottom- flange joint.

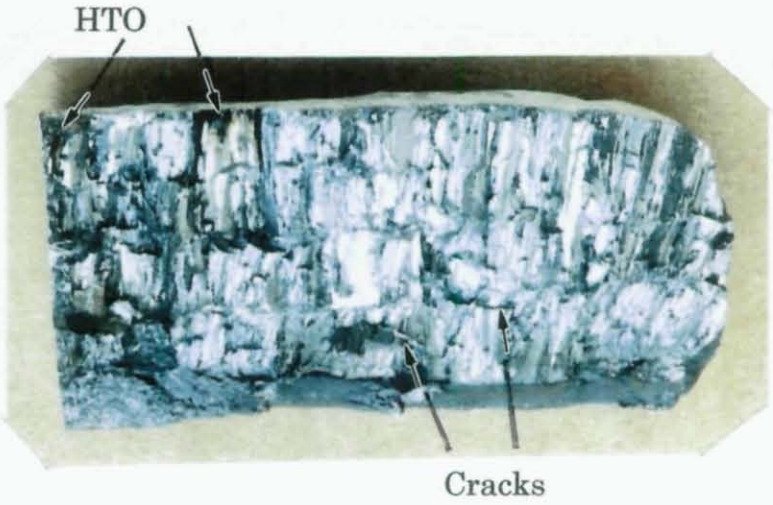

Figure 10. Fracture surface of the north end from the west-beam bottom-flange joint.

a)

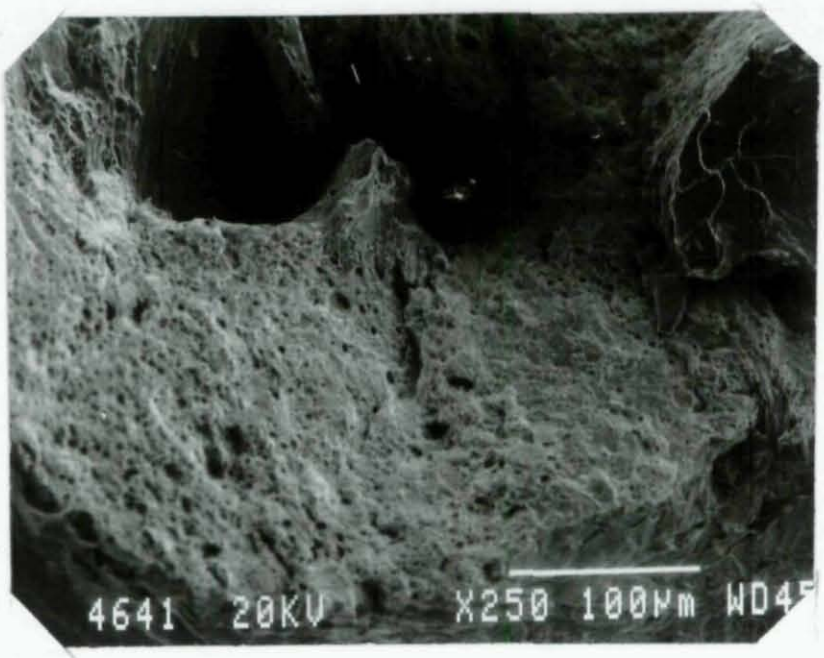

b)

Figure 11. Examples of ductile fractures in the west-beam bottom-flange joint.

(a) Macro section M1

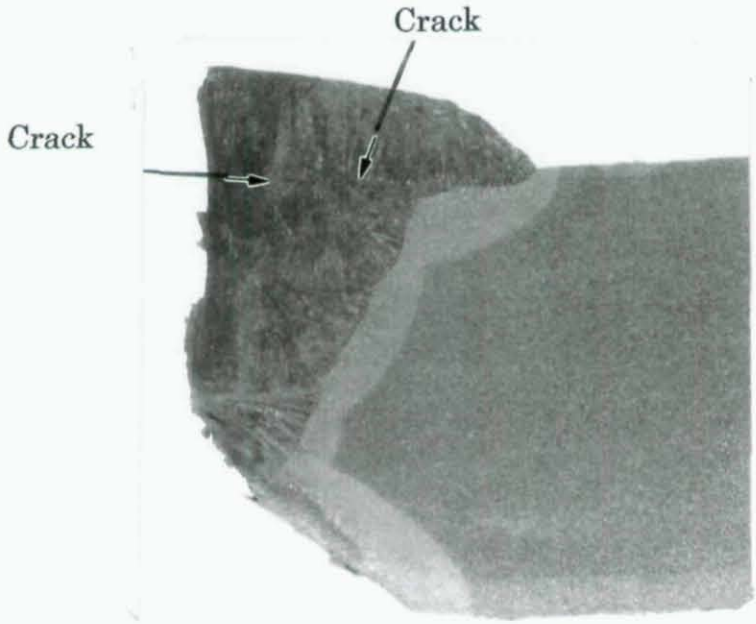

(b) Macro section M2

Figure 12. Macro sections from the west-beam bottom-flange joint.

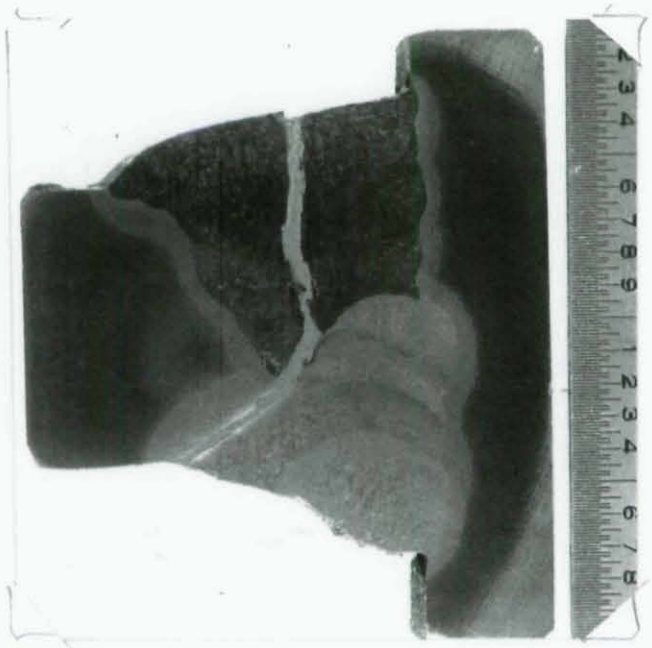

(a)

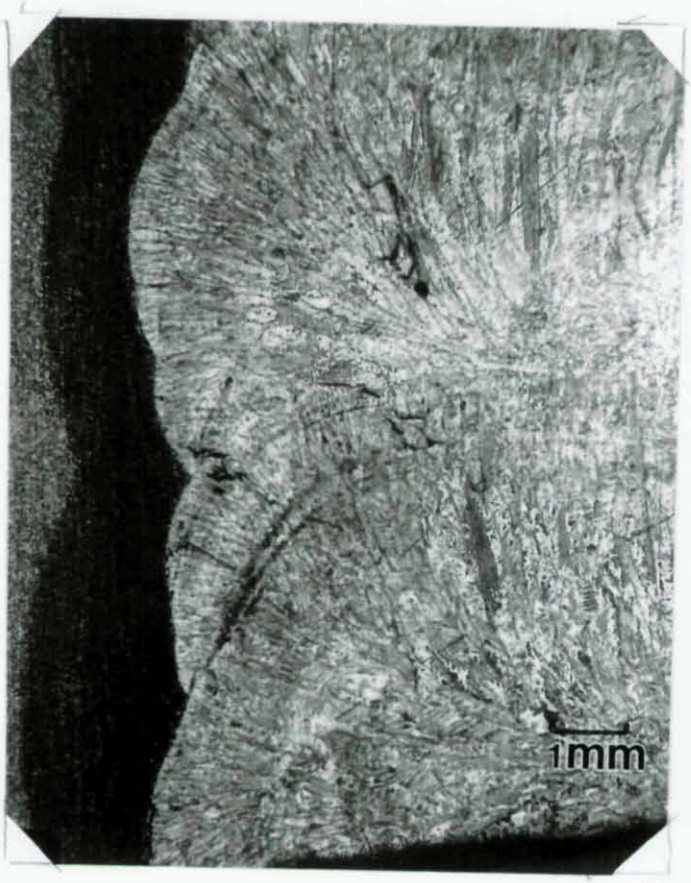

(b) 10X.

(c) 10X

Figure 13. Macro sections from the west-beam bottom-flange joint.

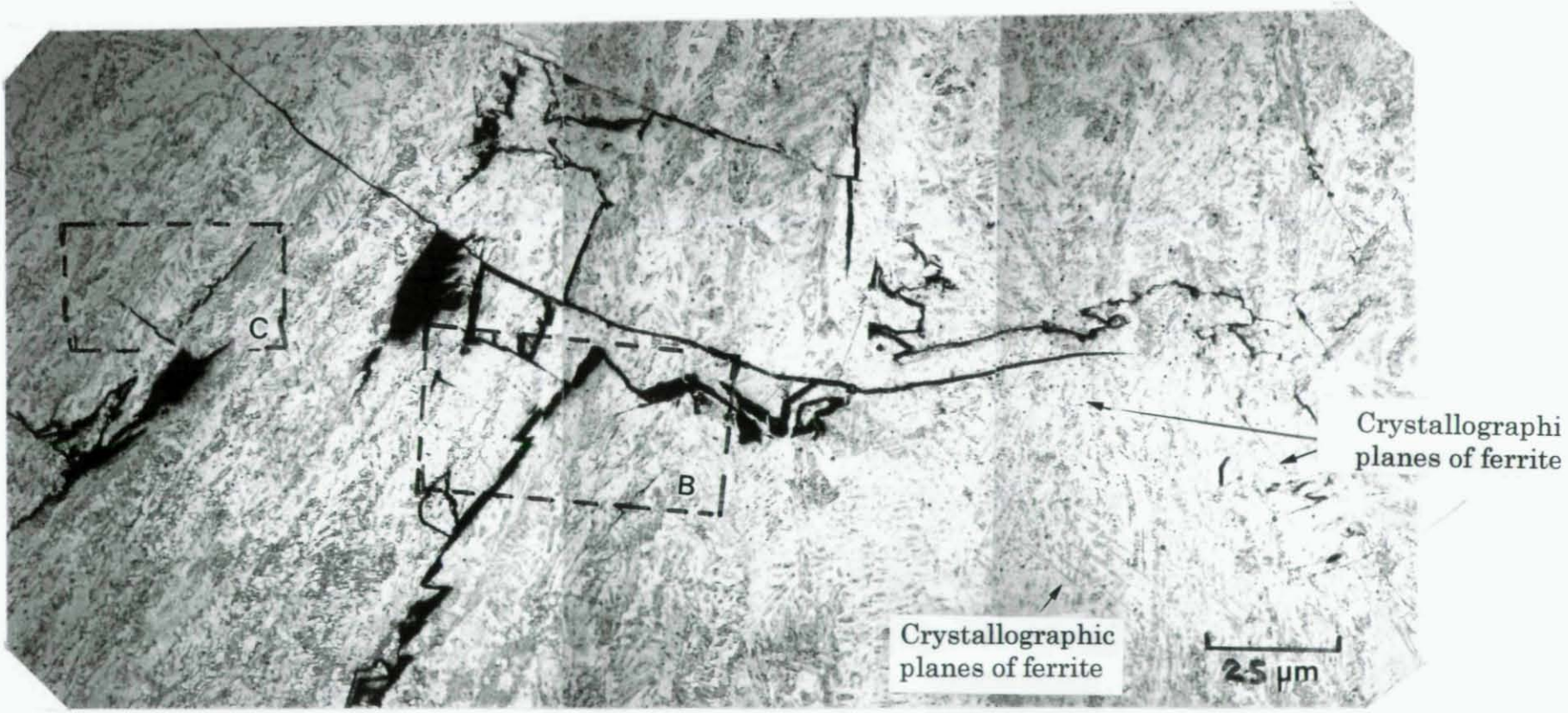

Figure 14. Cracks and crystallographic planes in ferrite in the deposited weld metal of the west-beam bottom-flange joint (enlarged area A in Figure 13-c).

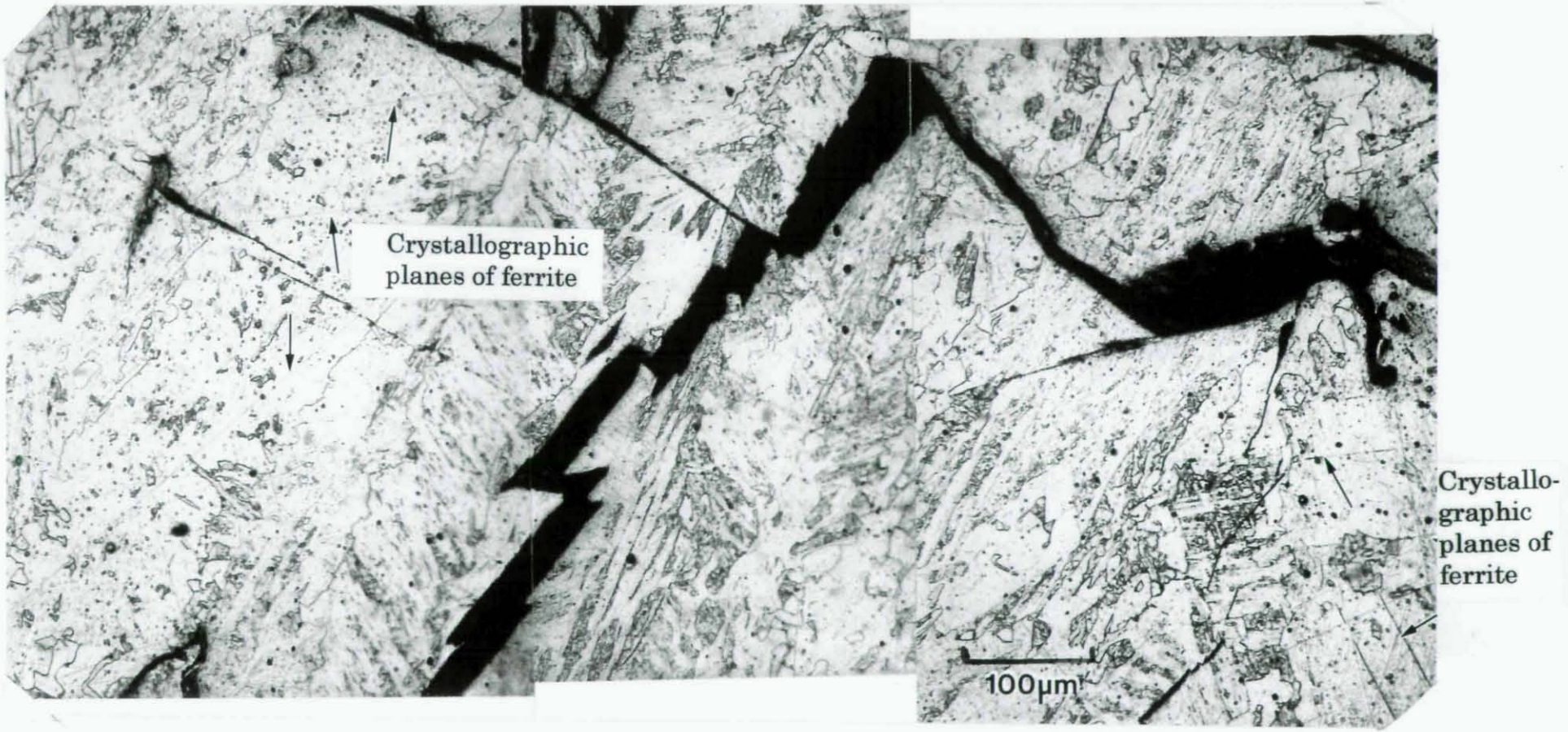

Figure 15. Cracks and crystallographic planes in ferrite in the deposited weld metal of the west-beam bottom-flange joint (enlarged area B in Figure 14).

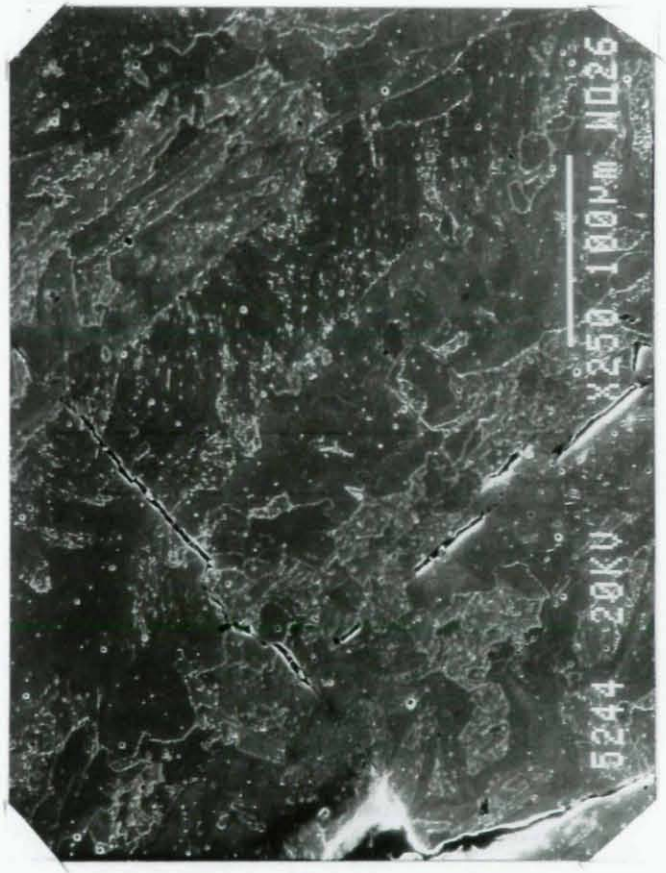

a)

b)

Figure 16. Cracks in the weld metal of the west-beam bottom-flange joint (enlarged area C in Figure 14).

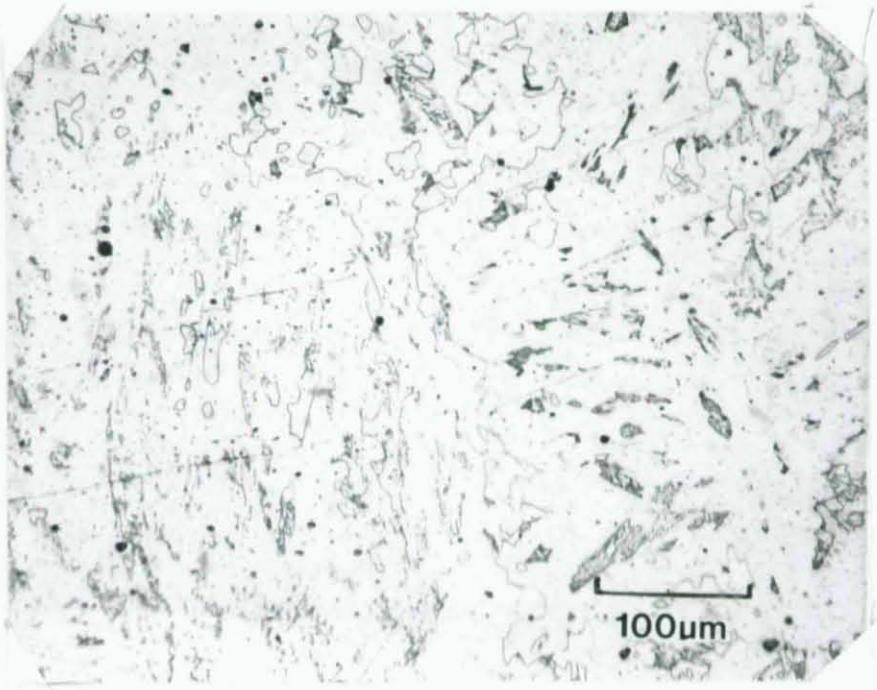

a)

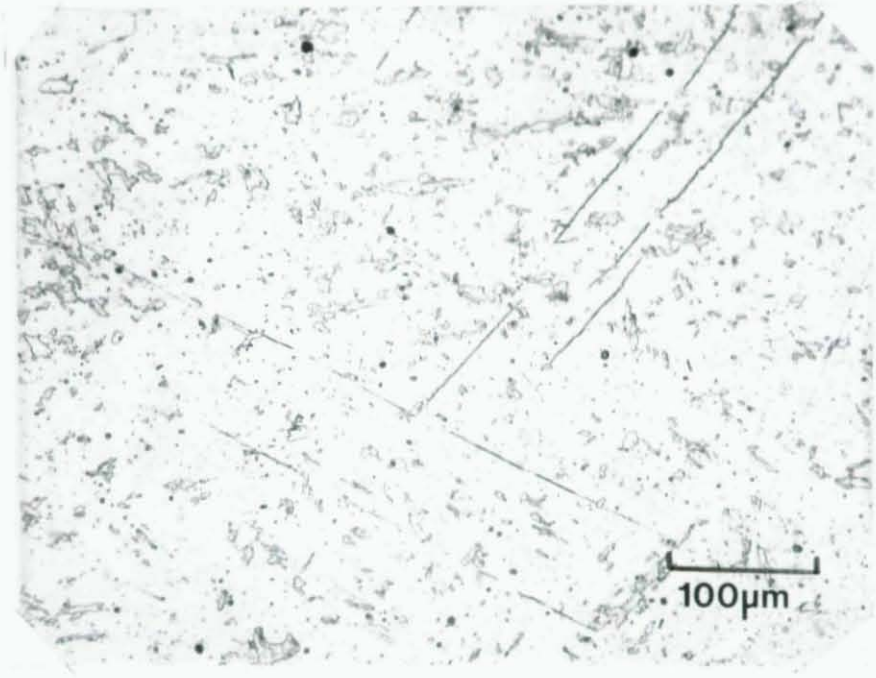

b)

Figure 17. Intersecting crystallographic planes at different stages of development. 200X.

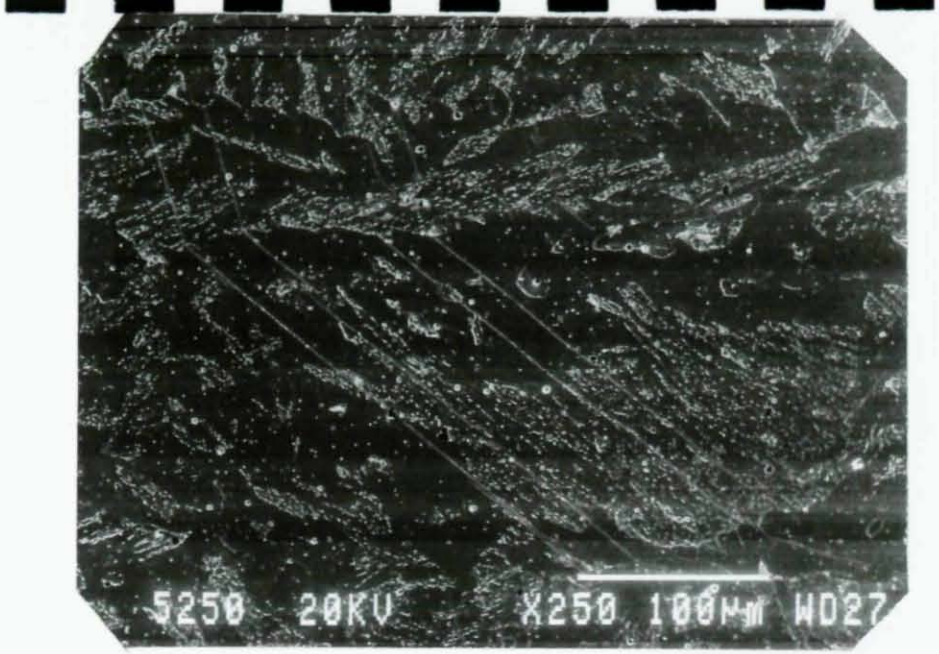

a)

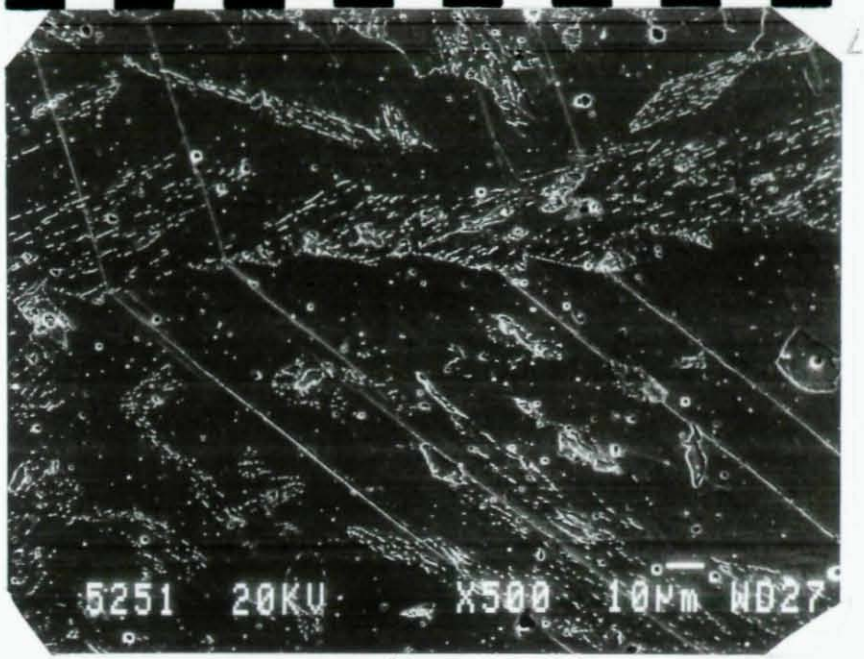

b)

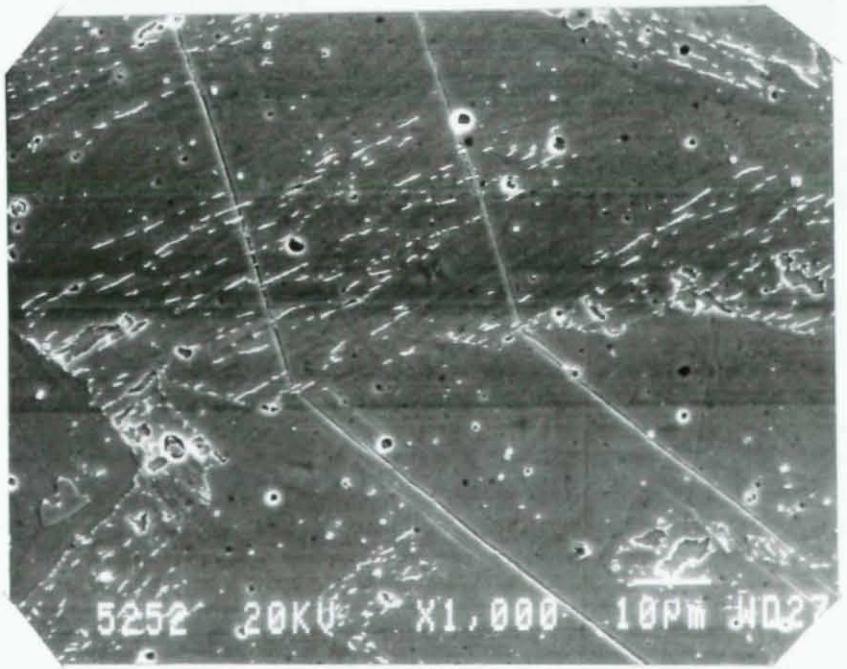

c)

Figure 18. A cluster of intersecting crystallographic planes at different magnifications.

Figure 19. Fractured east-beam top flange.

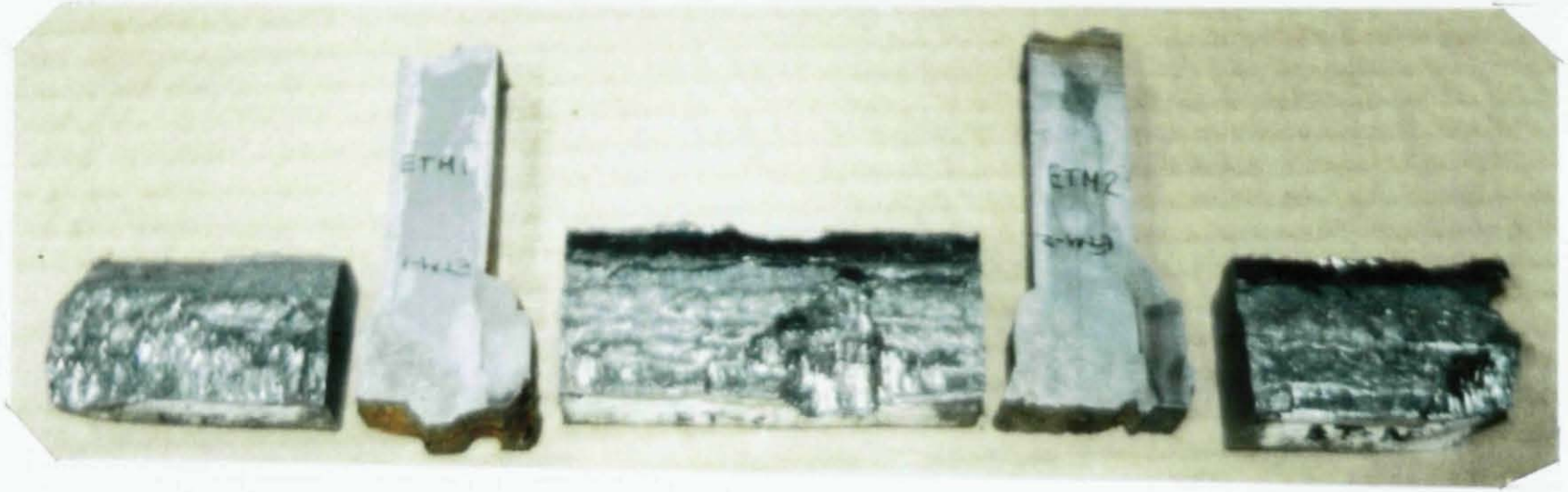

a)

b)

Figure 20. As received fracture pieces from the east-beam top-flange joint.

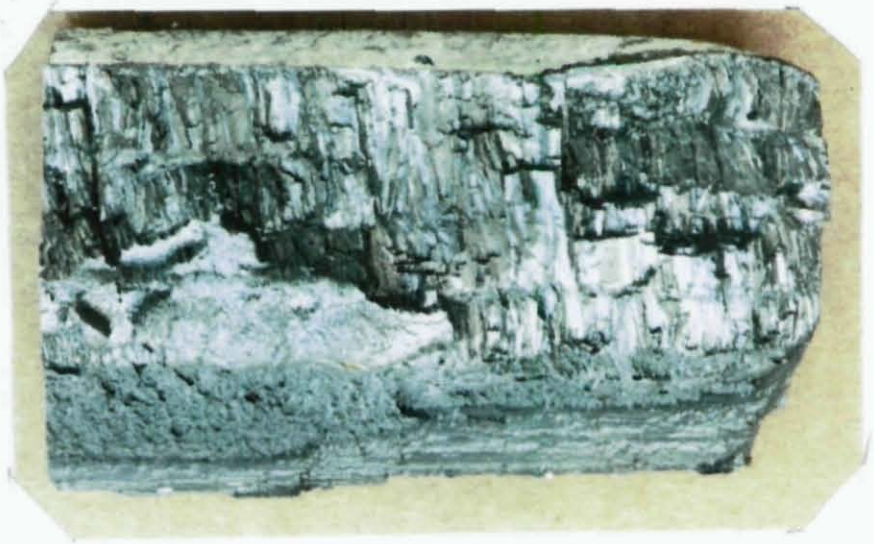

Figure 21. South piece from the beam-side fracture of the east-beam top-flange joint.

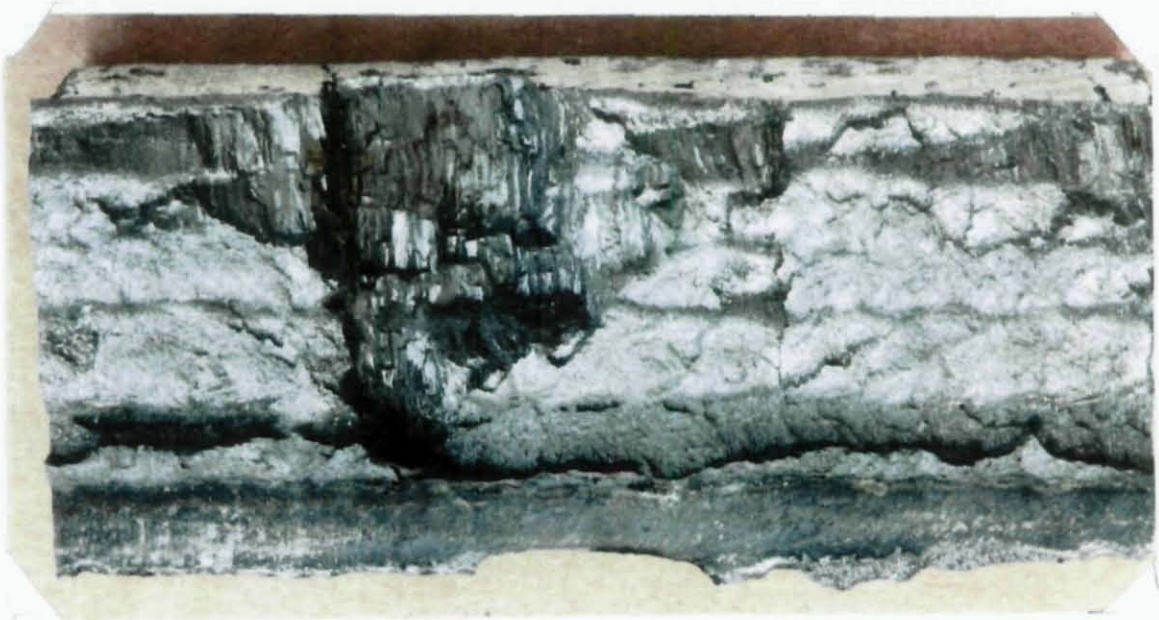

Figure 22. Center piece from the beam-side fracture of the east-beam top-flange joint.

Figure 23. North piece from the beam-side fracture of the east-beam top-flange joint.

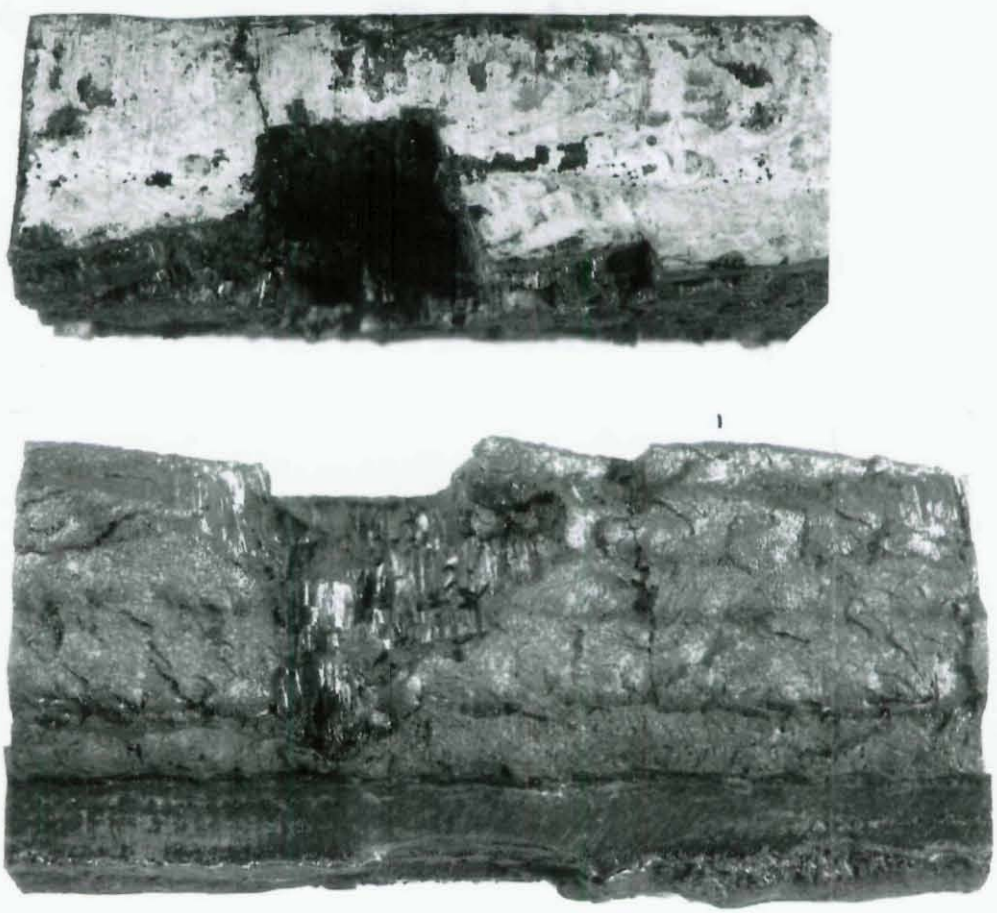

Figure 24. A wedge of weld metal separated from the center piece of the beam side fracture surface of the east-beam top-flange surface.

Figure 25. Boundary between weld-metal and fusion-plane fracture surfaces.

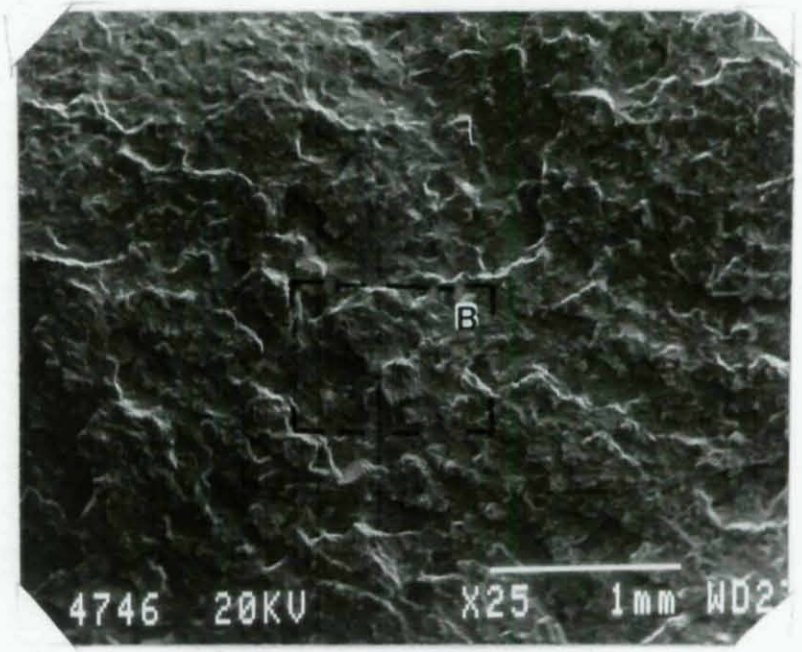

a) Enlarged area A in Figure 25.

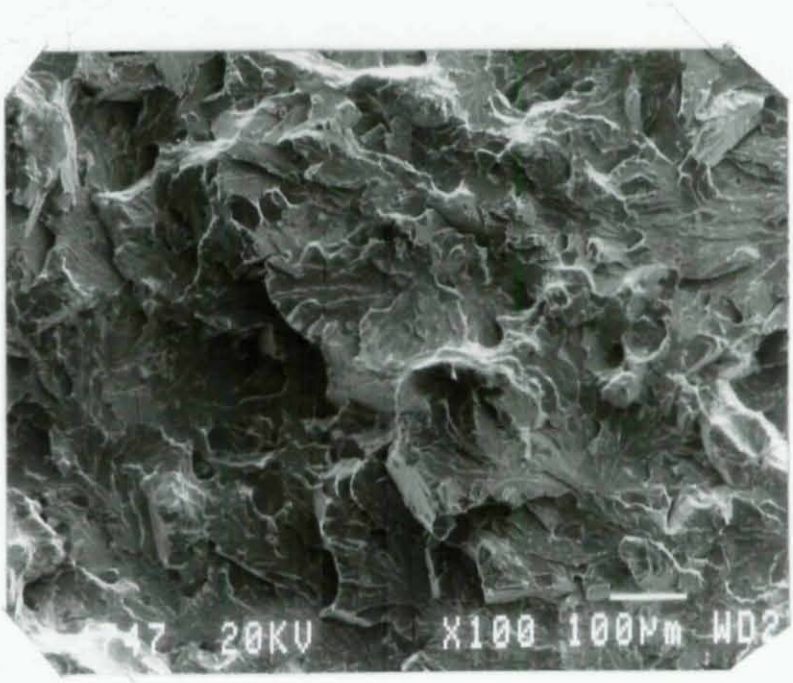

b) Enlarged area B in a (above).

Figure 26. Cleavage fracture along the fusion plane on the column-side fracture surface of the east-beam top-flange joint.

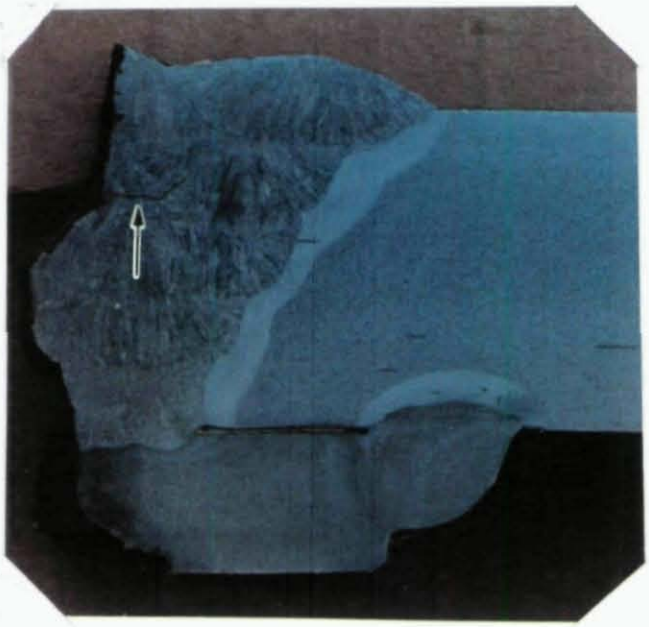

a) Macro section M1

b) Macro section M2

Figure 27. Macro sections from the east-beam top-flange joint.

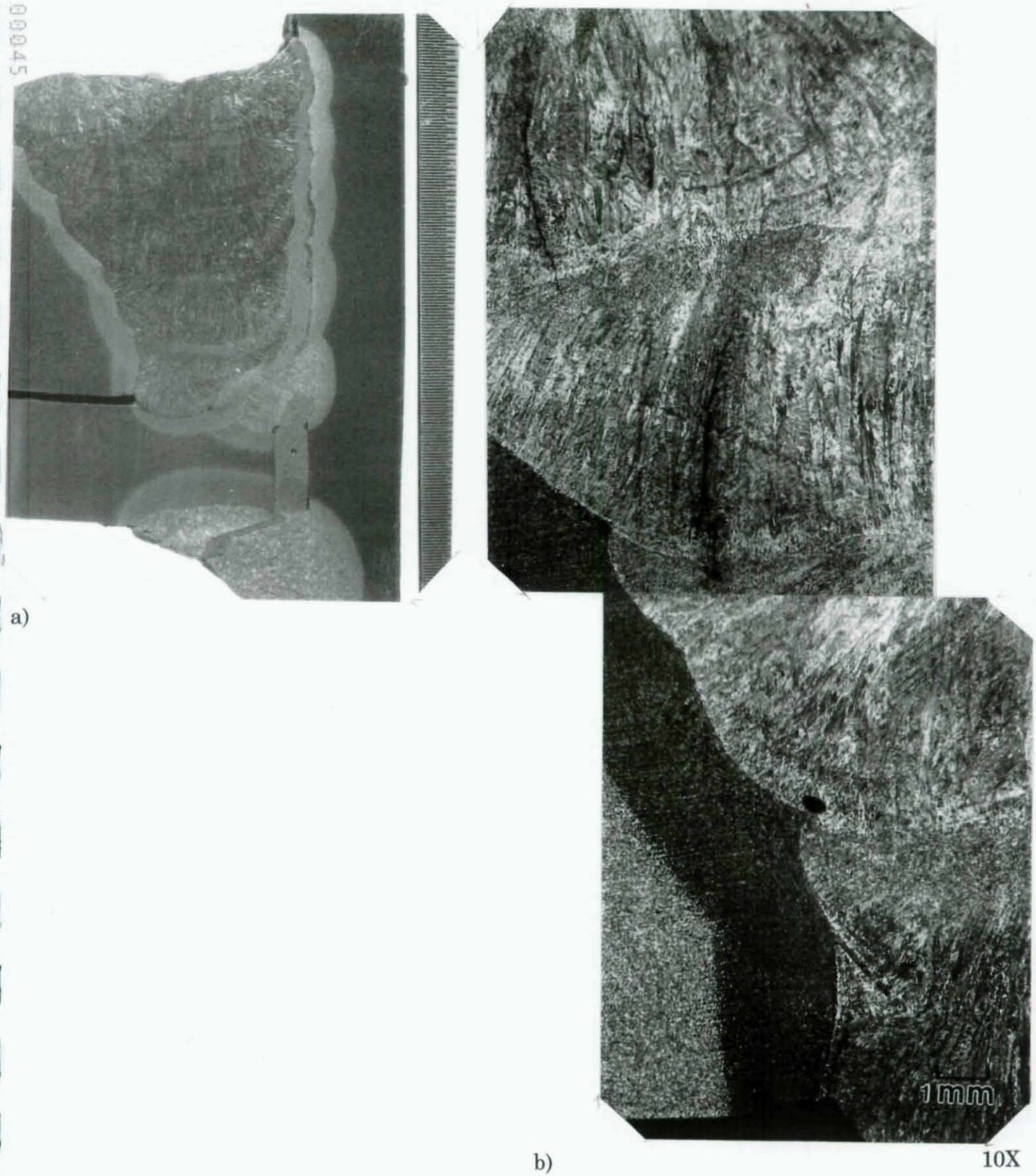

Figure 28. Macro section across the east-beam top-flange joint.

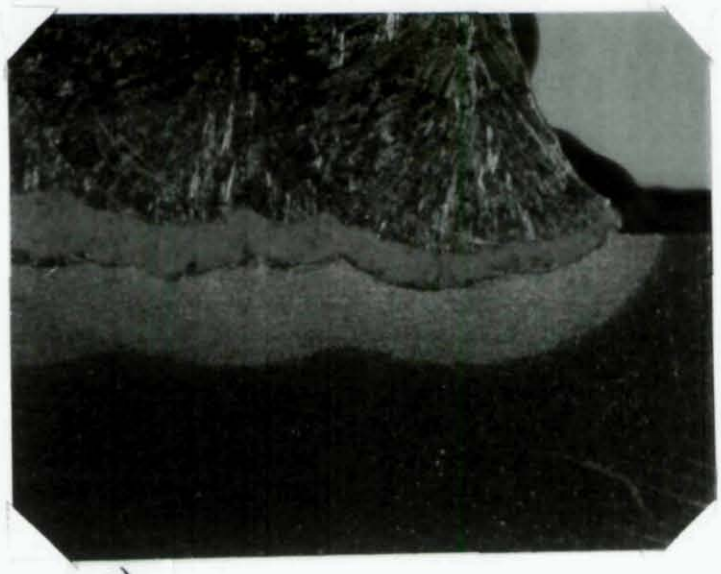

a)

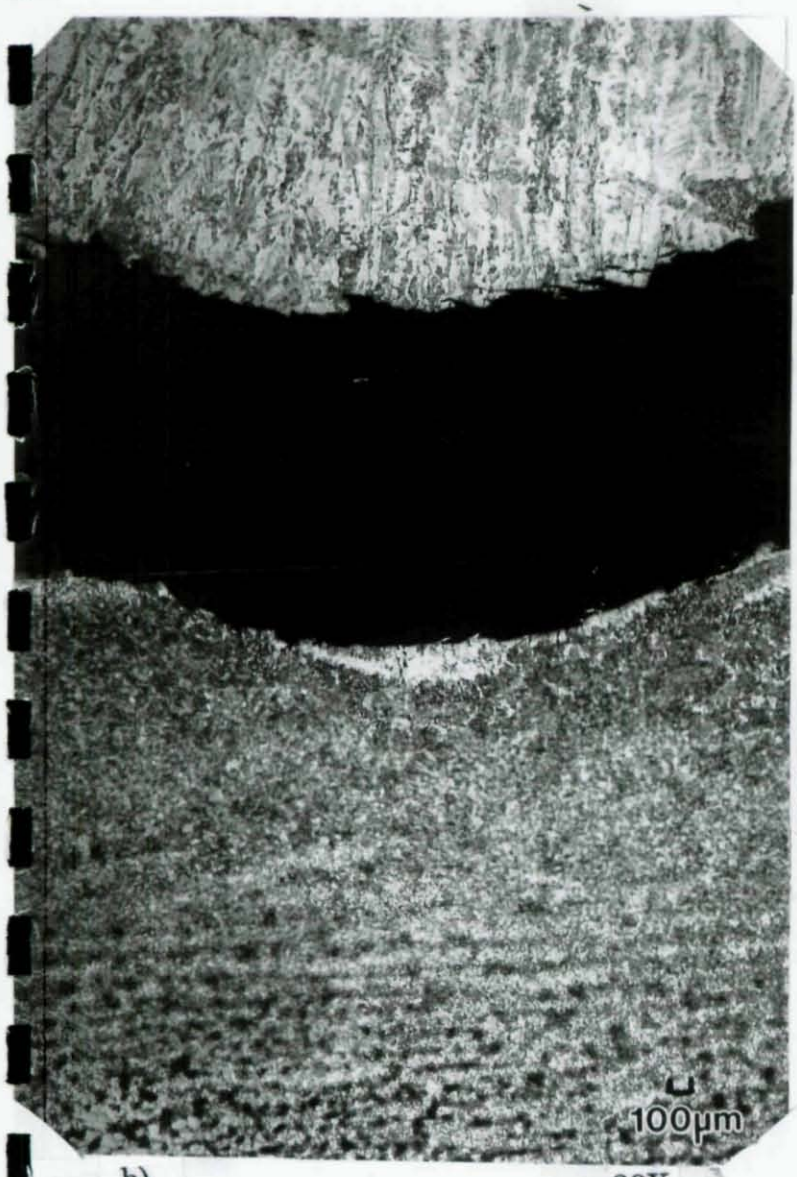

b) 30X

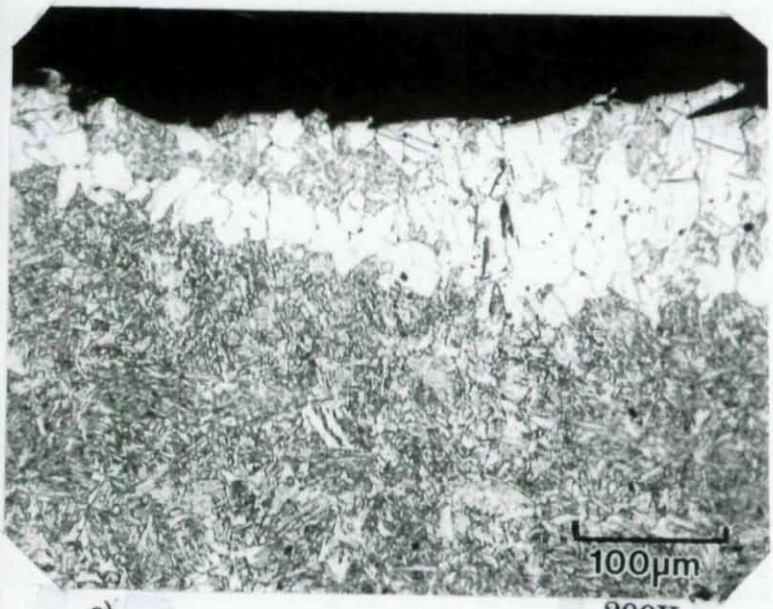

c) 200X

Figure 29. Close up of the fracture along the fusion plane in the east-beam top-flange joint.

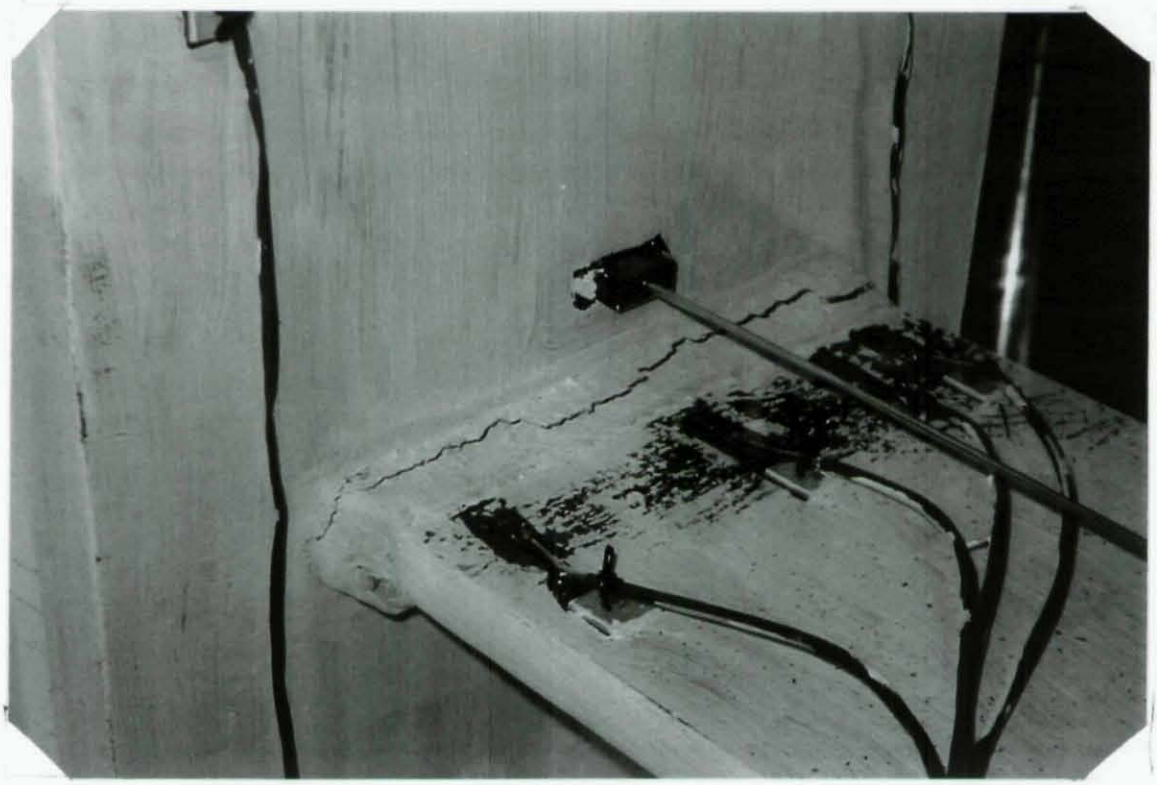

Figure 30. Fractured west-beam top flange.

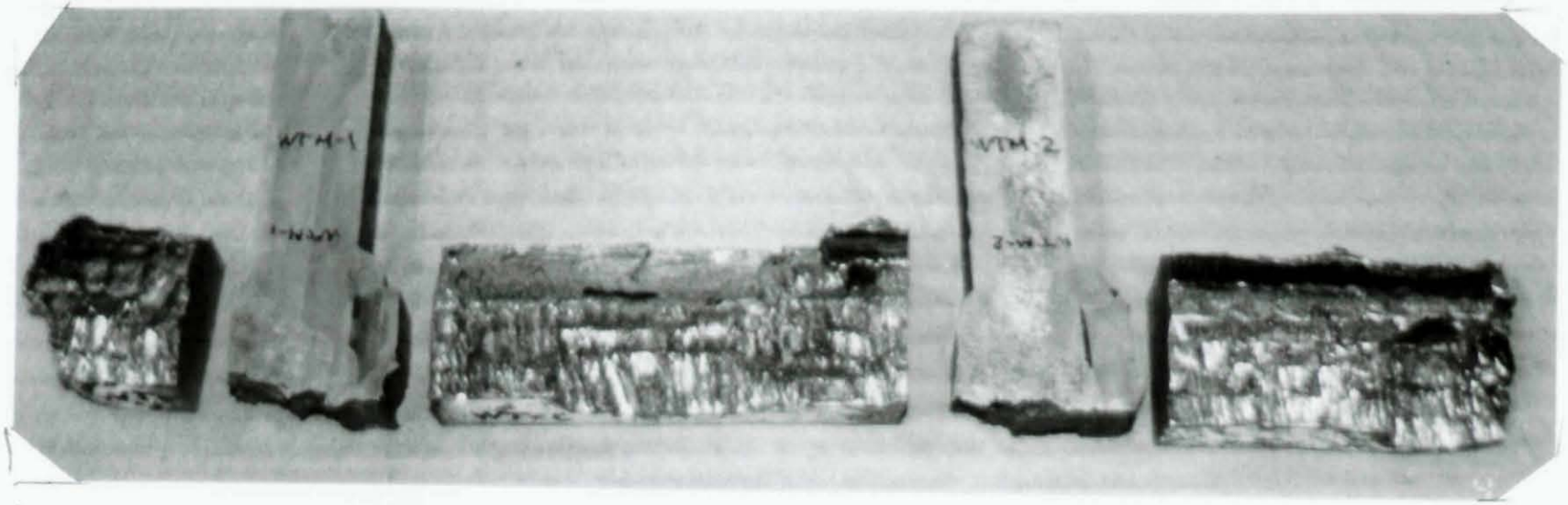

a)

b)

Figure 31. As received fracture pieces from the west-beam top-flange joint.

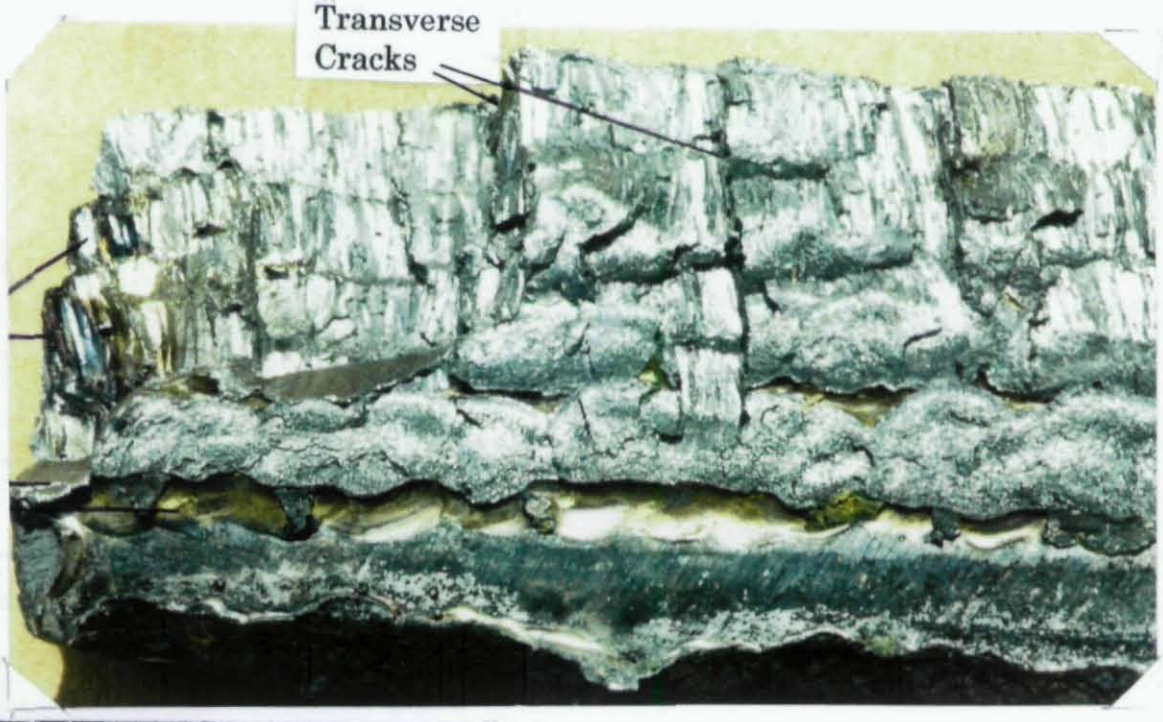

a)

b)

Figure 32. South piece from the beam-side fracture surface of the west-beam top-flange joint.

a)

b)

Figure 33. Center piece from the beam-side fracture surface of the west-beam top-flange joint.

a)

b)

Figure 34. An example of discontinuous cracks on crystallographic planes in ferrite.

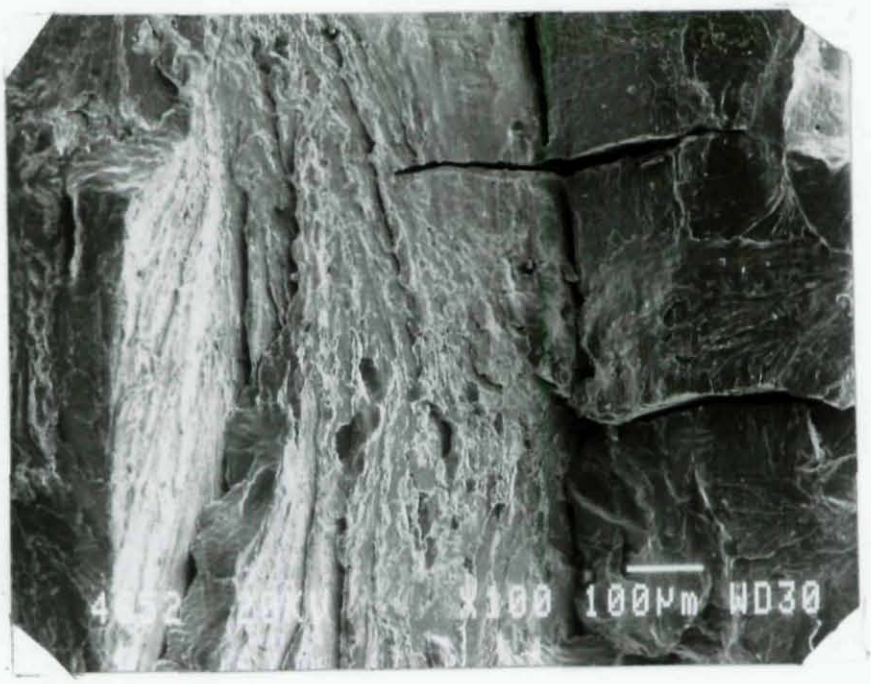

c)

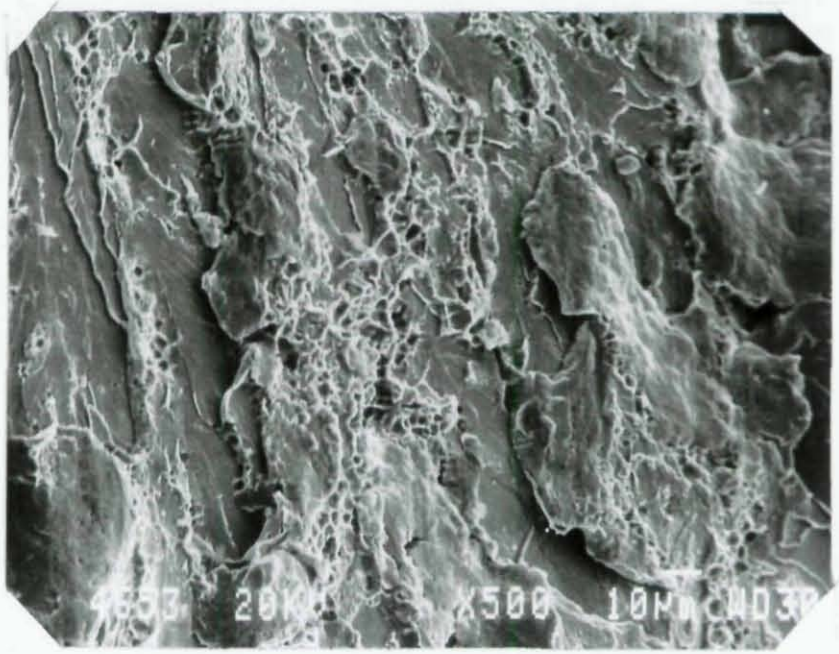

d)

Figure 34 (continued). An example of discontinuous cracks on crystallographic planes in ferrite.

a)

b)

Figure 35. North piece from the fracture surface on the beam side of the west-beam top-flange surface.

a) Macro section M1

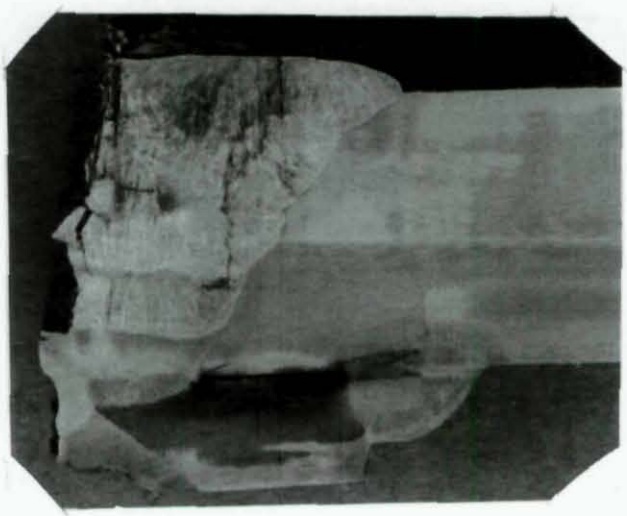

b) Macro section M2

Figure 36. Macro sections from the west-beam top-flange joint.

a)

b)

Figure 37. Macro section across the west-beam top-flange joint.

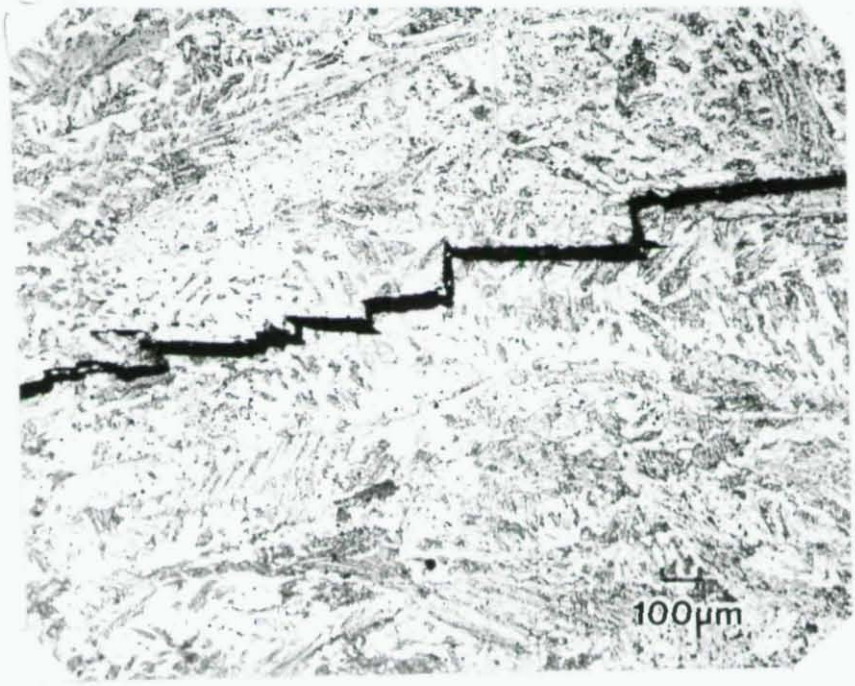

a) 50X

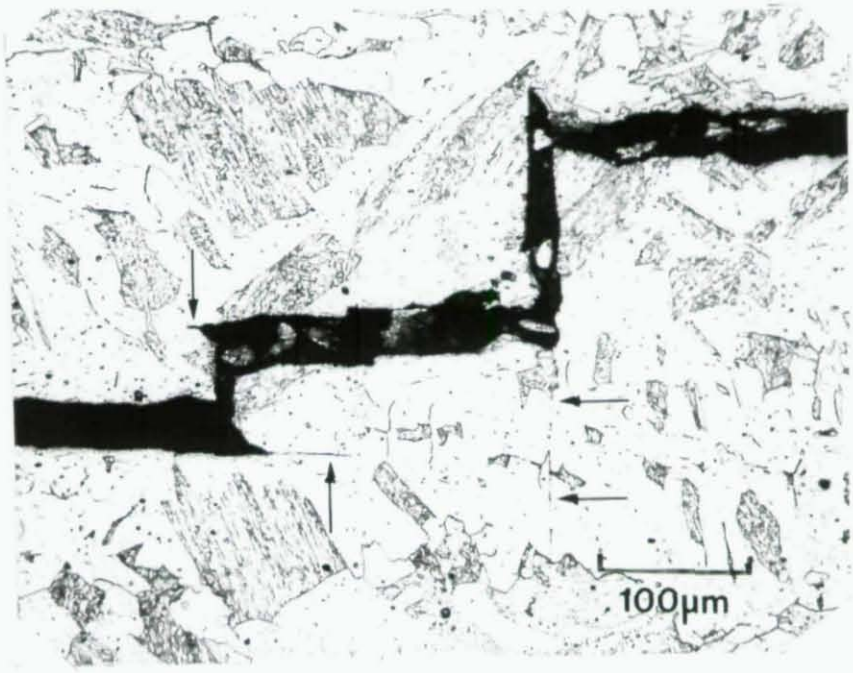

b) 200X

Figure 38. Step crack on a cross section from the west-beam top-flange joint.

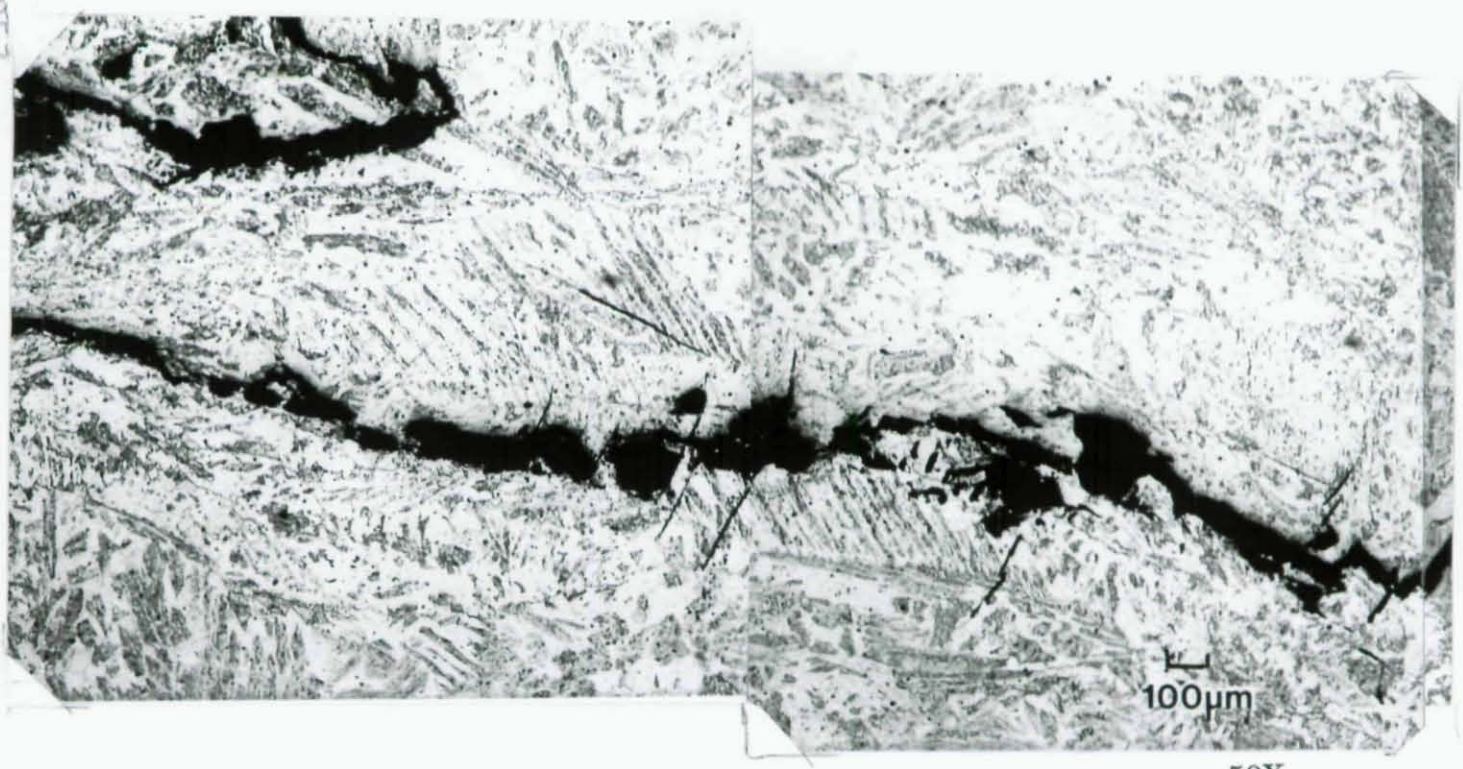

a) 50X

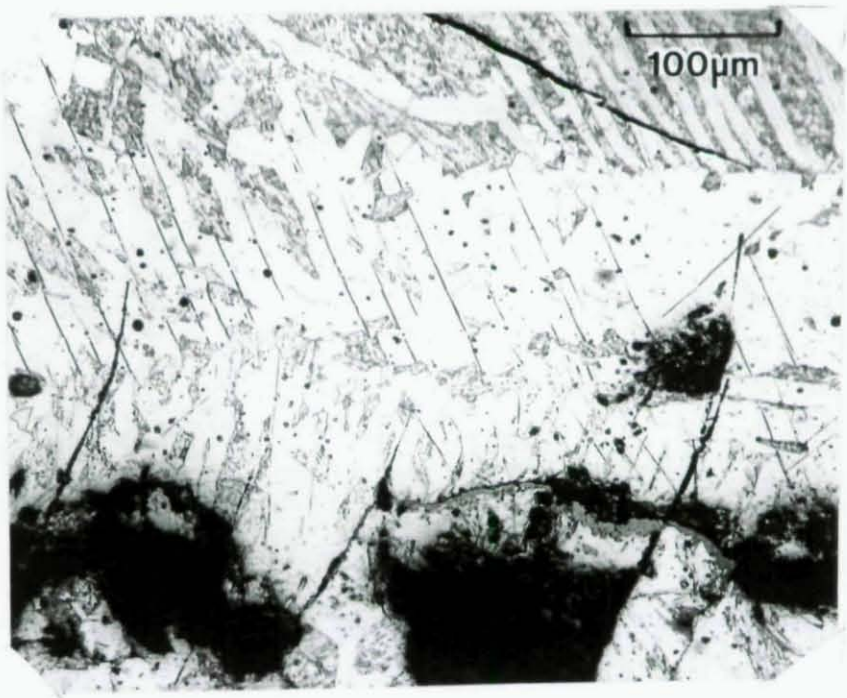

b) 200X

Figure 39. A meandering crack in a cross section from the west-beam top-flange joint.

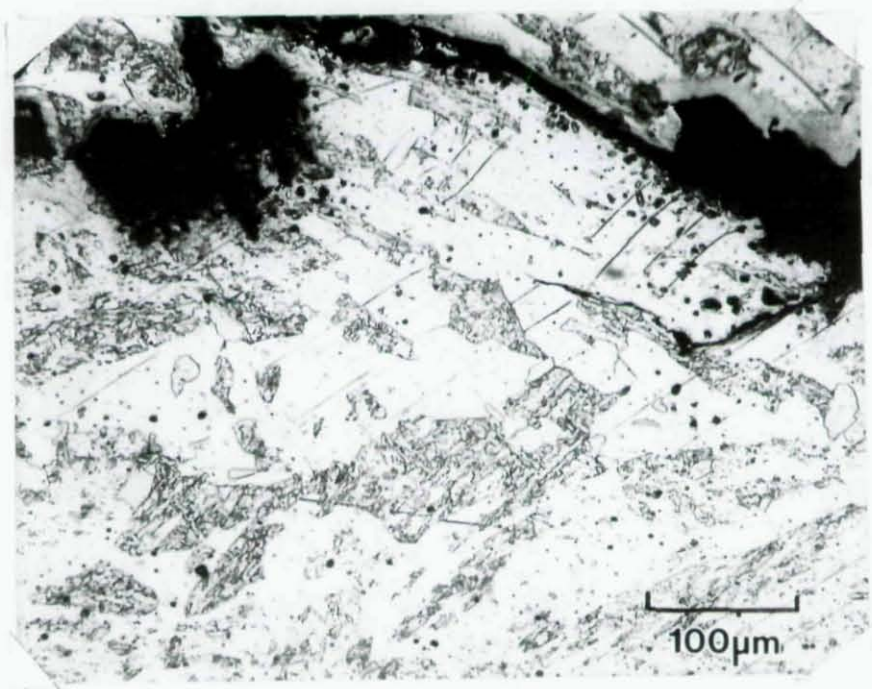

c)

Figure 39 (continued). A meandering crack in a cross section from the west-beam top-flange joint.

Figure 40. Cracks emanating from a conditioned area on the top surface of the deposited weld metal in the west-beam bottom-flange.